nature communications

Article

https://doi.org/10.1038/s41467-024-53060-4

Inhibition of neutrophil swarming by type I interferon promotes intracellular bacterial evasion

Received: 10 November 2023

Accepted: 27 September 2024

Published online: 07 October 2024

Check for updates

Shimin Li[1], Qi Yao[2], Jiajia Li[2], Haoxiang Yang[3], Rui Qian[4], Meijuan Zheng[4], Ning Wu[5], Hongyuan Jiang[3], Lu Li[1,6] ✉ & Zhutian Zeng[1,2,6] ✉

Listeria monocytogenes (LM) possesses the ability to breach multiple barriers and elicit intricate immune responses. However, there remains a lack of explicit understanding regarding how LM evades innate immune surveillance within the body. Here, we utilized liver intravital imaging to elucidate the dynamic process of LM during infection in the liver. We discovered that LM can rapidly escape from Kupffer cells (KCs) through listeriolysin O (LLO) and proliferate within hepatocytes. Upon LM exposure to the hepatic sinusoids, neutrophils rapidly aggregate at the site of infection. Subsequently, LM can induce type I interferon (IFN-I) production primarily in the spleen, which acts systemically on neutrophils to hamper their swarming by deactivating the ERK pathway, thus evading neutrophil-mediated eradication. Furthermore, our findings suggest that virus-induced IFN-I suppresses neutrophil swarming, and COVID-19 patients exhibit impaired neutrophil aggregation function. In conclusion, our findings provide compelling evidence demonstrating that intracellular bacteria represented by LM can hijack host defense mechanisms against viral infections to evade immune surveillance. Additionally, impaired neutrophil swarming caused by IFN-I is one of the significant factors contributing to the increased susceptibility to bacterial infections following viral infections.

Listeria monocytogenes (LM) is a gram-positive intracellular bacterium and a foodborne pathogen that can trigger both systemic innate and adaptive immune responses upon infection[1]. It serves as a valuable model bacterium for studying immune responses to bacterial infections due to its ability to penetrate host barriers and survive intracellularly. While the interaction mechanisms between LM and host cells have been well understood at the cellular level[2], in vitro systems are often too simplistic to capture the complexity of in vivo infections. Consequently, there is still a lack of clear understanding regarding the dynamic changes that occur during LM in vivo infection, particularly in terms of how LM evades pursuit and containment by various cells of the innate immune system.

Liver resident macrophages, known as Kupffer cells (KCs), are responsible for capturing LM in the blood[3]. LM employs a variety of mechanisms to escape from macrophages during in vitro infection. For instance, it utilizes LLO (Listeriolysin O) to perforate the phagosomal membrane, enabling its escape into the cytoplasm. Once inside the cytoplasm, LM relies on ActA to facilitate its cell-to-cell spread[4,5].

[1]Department of Oncology, The First Affiliated Hospital of USTC, Division of Life Sciences and Medicine, University of Science and Technology of China, Hefei, China. [2]Key Laboratory of Immune Response and Immunotherapy, Center for Advanced Interdisciplinary Science and Biomedicine of IHM, School of Basic Medical Sciences, Division of Life Sciences and Medicine, University of Science and Technology of China, Hefei, China. [3]CAS Key Laboratory of Mechanical Behavior and Design of Materials, Department of Modern Mechanics, CAS Center for Excellence in Complex System Mechanics, University of Science and Technology of China, Hefei, China. [4]Department of Clinical Laboratory, First Affiliated Hospital of Anhui Medical University, Hefei, China. [5]The First Affiliated Hospital of Anhui Medical University and Institute of Clinical Immunology Anhui Medical University, Hefei, China. [6]These authors jointly supervised this work: Lu Li, Zhutian Zeng. ✉e-mail: lilu@ustc.edu.cn; zengzt@ustc.edu.cn

However, in contrast to an environment composed solely of macrophages in vitro, the body contains numerous parenchymal cells that have a limited capacity to defend against bacterial infections, such as hepatocytes. Therefore, the mechanisms by which LM evades KCs need to be further investigated. Furthermore, although other innate immune cells, such as neutrophils, have been reported to be recruited to infected tissues during LM infection, the mechanisms of their interaction with LM remain unclear[6]. Neutrophils play a significant role in the rapid response to microbial infections[7]. Recent advancements in intravital imaging techniques have improved our understanding of neutrophils. Neutrophils that infiltrate local tissue can be activated by stimuli from pathogens or dead cell debris, leading to neutrophil swarming[8], where neutrophils activate and aggregate to engulf pathogens and promote their clearance[9]. Therefore, it is essential to redefine the role and mechanisms by which neutrophils contribute to resistance against LM infection.

Type I interferons (IFN-I) are a subset of interferon proteins that play a crucial role in modulating both innate and adaptive immune responses during viral and bacterial infections[10–12]. Previous studies have reported that IFN-I impairs the clearance of intracellular bacteria, such as LM[13], *Mycobacterium tuberculosis*[14], and *Francisella tularensis*[15]. Mechanistically, IFN-I suppresses phagosome maturation and the proteolysis of LM virulence factors ActA and LLO through IFITM3, promoting phagosome escape and cell-to-cell spread[16,17]. It also inhibits the activation of phagocytes by downregulating IFN-γ receptor expression[18]. While some studies have reported that IFN-I negatively regulates chemokine signaling and modulates neutrophil recruitment[19,20], it remains elusive whether and how IFN-I directly affects neutrophil behavior and function[21].

Almost all viral infections induce an upregulation of IFN-I expression and IFN-I is the main effector cytokine of the host immune response against viral infections[11]. It has been reported that several viruses can promote secondary bacterial infections[22,23]. These intracellular bacteria, like viruses, undergo cytoplasmic growth processes, and they also induce the expression of IFN-I through intracellular pathways[11]. Therefore, we speculate that intracellular bacterial infections can create an environment similar to viral infections, to some extent, thereby helping them evade immune surveillance. Hence, elucidating the mechanisms by which intracellular bacteria evade immune surveillance may help uncover the mystery of how viral infections promote secondary bacterial infections.

In this study, we utilized intravital imaging to provide a comprehensive description of the infection process of LM in the liver. Our findings demonstrate that LM employs LLO to perforate the KC membrane, allowing it to escape back into the liver sinusoids, rather than relying on ActA for cell-to-cell dissemination. Subsequently, the LM that infects hepatic parenchymal cells undergoes significant amplification under the protection of these cells. Notably, the partial death of KCs resulting from membrane perforation does not trigger neutrophil swarming. Only after hepatocyte lysis, when LM is exposed to the hepatic sinusoids and continuously stimulates neutrophils, can it eventually induce neutrophil swarming. However, our research has revealed that LM-induced IFN-I in the spleen has the capability to suppress neutrophil swarming by deactivating the ERK pathway, thereby aiding LM in evading the detrimental effects of neutrophils. Furthermore, we observed that the detrimental effect of IFN-I on neutrophils plays a role in virus-induced secondary bacterial infections.

Results

LM escapes from KCs by relying on LLO-mediated perforation of the cell membrane

To investigate how LM evades the innate immune system in vivo, we initially examined the organ distribution following LM infection. Consistent with previous reports, more than 90% of LM was sequestered in the liver (Fig. 1a). KCs play a pivotal role in filtering pathogens from the bloodstream[24]. Through time-lapse imaging, we observed rapid uptake of LM almost exclusively by F4/80$^+$ KCs (Fig. 1b), confirming the important role of KCs in filtering circulating LM. Despite the retention of LM within KCs at 90 min post-infection, we observed KCs being stained with PI (propidium iodide), a cell impermeable DNA dye, indicating that the cell membrane of KCs had been damaged (Fig. 1c and Movie S1). Subsequently, we found that LM escaped from these damaged KCs and re-entered the hepatic sinus rather than infecting neighboring cells (Fig. 1c and Movie S1). Previous studies suggested that LM spreads between neighboring cells in an ActA-dependent manner in vitro[4]. However, upon ActA-deficient LM (LM-Δ*actA*) infection, we still observed damage of KC cell membranes at 90 min and subsequent escape and re-entry of LM into the hepatic sinus, consistent with wild-type (WT) LM (Fig. 1d and Movie S1). LLO plays an important role in the escape of LM from the lysosome to the cytoplasm[2], thus we wondered whether LLO is involved in the escape of LM to the extracellular space. LLO-deficient LM (LM-Δ*hly*) infection did not cause damage to the cell membrane of KCs, as indicated by the absence of PI staining. Additionally, LM-Δ*hly* was unable to escape from KCs throughout the period of observation (Fig. 1e and Movie S1). In line with these findings, LLO deficiency rendered LM susceptible to rapid clearance in the liver, while ActA deficiency did not significantly impact the infectivity of LM (Fig. 1f). In summary, these results indicate that during in vivo infections, LM relies on LLO-mediated perforation of KC membranes for escape and dissemination.

Neutrophil swarming is indispensable for controlling the early spread of LM

Neutrophils are an essential component of the host's innate immune defense against bacteria, and previous reports have indicated that neutrophils are rapidly recruited to the infected tissues after LM infection[6]. Therefore, we wondered how neutrophils play a role in LM infection in the liver. We observed that escaped LM started infecting hepatocytes and proliferated extensively within them at 6 h post-infection. Notably, despite neutrophils being recruited to the liver at this time, they were unable to detect the presence of LM hiding within the hepatocytes (Fig. 2a and Movie S2). On the other hand, consistent with the previous study, LM infection resulted in the death of KCs[25], and we observed the formation of transient neutrophil aggregates around the fragmented dead KCs (Fig. 2a and Movie S2). Although cell death can induce neutrophil swarming, it has been reported that tissue-resident macrophages can shield small wounds to terminate neutrophil swarming, preventing unnecessary tissue damage[26]. Subsequent imaging revealed that extensive LM proliferation led to hepatocyte lysis, exposing LM again in the hepatic sinus, which caused rapid neutrophil aggregation at the site of infection (Fig. 2b and Movie S3). In summary, taking advantage of liver intravital imaging, we delineated the early stages of LM infection, which involve initial capture by KCs, subsequent escape from KCs and infection of hepatocytes, and ultimately, hepatocyte lysis and induction of neutrophil swarming (Fig. 2c).

To further investigate whether neutrophil swarming is involved in the clearance of intracellular bacteria, we compared LM infection with that of extracellular bacterial strain *Staphylococcus aureus* MW2 or uropathogenic *Escherichia coli* CFT073. MW2 and CFT073 were also primarily captured by KCs during infection (Supplementary Fig. 1a–d) and induced neutrophil infiltration into the liver, but they failed to elicit neutrophil swarming (Fig. 2d). Consistently, the depletion of neutrophils aggravates the LM infection, but does not affect the MW2 or CFT073 infection (Fig. 2e–g). In addition, inhibiting neutrophil swarming by Zileuton (Fig. 2h, i), an inhibitor of the enzyme 5-lipoxygenase (5-LOX) involved in leukotriene B4 (LTB4) synthesis, exacerbates LM infection (Fig. 2j). In conclusion, these results suggest that the activation and formation of neutrophil swarming play a role in restricting LM infection.

https://doi.org/10.1038/s41467-024-53060-4

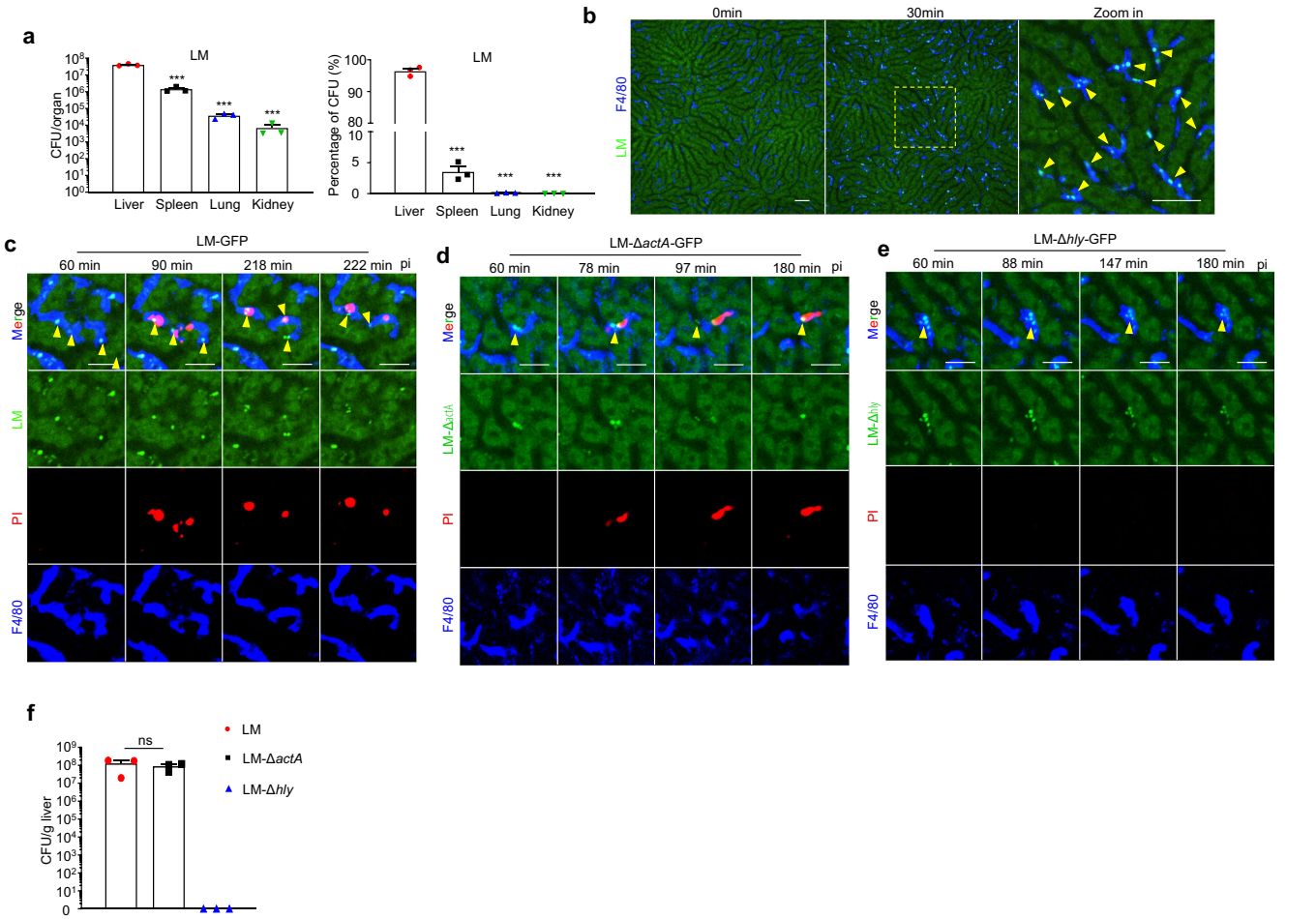

Fig. 1 | LM escapes from KCs by relying on LLO-mediated perforation of the cell membrane. a WT mice were intravenously infected with 1×10^8 CFU of LM-GFP. The bacterial load in the liver, spleen, lung, and kidney was assessed 30 min post-infection. Data were from three mice. ($P < 0.0001$). **b** Intravital images showing the capture of LM in the liver. APC anti-F4/80-labeled KCs (blue) and LM-GFP (green). Captured LM are indicated by yellow arrows. Scale bar, 50 μm. **c**–**e** Mice were infected with 1×10^8 CFU of the indicated LM strains intravenously. Dynamic intravital images showing the escape of LM-GFP (**c**), LM-Δ*actA*-GFP (**d**), and LM-Δ*hly*-GFP (**e**) from KCs. APC anti-F4/80-labeled KCs (blue), bacteria (green), and nucleic acid staining dye PI (red) are shown. Escaped LM are indicated by yellow arrows. Scale bar, 25 μm. **f** Mice were intravenously infected with 1×10^8 CFU of LM-GFP, LM-Δ*actA*-GFP or LM-Δ*hly*-GFP. The bacterial load in the liver was assessed 48 h post-infection. Data were from three mice in each group. Data are represented as mean ± SEM; ***$P < 0.001$; ns no significance.

Next, we aim to explore how neutrophil swarming limits LM infection. Time-lapse intravital imaging revealed intimate contacts between congregated neutrophils and LM at the infectious foci. Although distinguishing the dynamic process of bacterial capture by a single neutrophil was literally impossible, we noticed that some LM exhibited substantial motility inside neutrophil aggregates, suggesting that they were internalized by migrating neutrophils (Movie S3). This was confirmed by flow cytometric analysis showing that a proportion of neutrophils in the liver but not the blood had phagocytosed LM (Supplementary Fig. 2a). In line with this, live-cell imaging indicated that neutrophils can actively take up LM in vitro, and this process did not cause cell lysis in neutrophils as observed for KCs (Supplementary Fig. 2b). The production of reactive oxygen species (ROS) is crucial for neutrophil-mediated bacterial killing upon phagocytosis[27]. Accordingly, we observed a significant upregulation of ROS production in neutrophils from the liver of LM-infected mice (Supplementary Fig. 2c), as well as in bone marrow neutrophils stimulated with LM in vitro (Supplementary Fig. 2d). Moreover, treatment of mice with Setanaxib, a selective inhibitor of the NADPH oxidase 1 and 4 (NOX1/4) that drive ROS production[28], exacerbated LM replication in the liver (Supplementary Fig. 2e). Notably, neutrophil extracellular traps (NETs), which represent an effective anti-microbial activity of neutrophils that is primarily triggered by ROS[29], were not detected at sites of neutrophil swarming (Supplementary Fig. 2f). Consistently, pharmacological inhibition of or genetic deficiency in peptidylarginine deiminase 4 (PAD4), which is required for NETs production[30], did not impact hepatic burden of LM (Supplementary Fig. 2g, h). These data collectively suggest that neutrophils swarmed towards the infectious foci, phagocytosed LM that escaped from dying hepatocytes and killed LM in a ROS-dependent but NETs-independent manner.

In addition to direct microbial killing, neutrophil swarming may help confine the spread of LM by causing bystander death of uninfected hepatocytes. In the mT/mG reporter mice which ubiquitously express tdTomato on the cell membrane, we serendipitously found that neutrophils had no discernable tdTomato expression compared to hepatocytes in our intravital imaging settings (Supplementary Fig. 3a). This allowed us to dynamically visualize and distinguish the death of hepatocytes at sites of neutrophil aggregates. Our results showed that both LM-infected and adjacent uninfected hepatocytes underwent rapid membrane rupture (Supplementary Fig. 3b), confirming the bystander cytotoxic effects mediated by neutrophil swarming. Consequently, damaged liver parenchymal areas largely overlapped with neutrophil clusters and extended well beyond LM-infected hepatocytes at 24 h post-infection. Depletion of neutrophils remarkably

https://doi.org/10.1038/s41467-024-53060-4

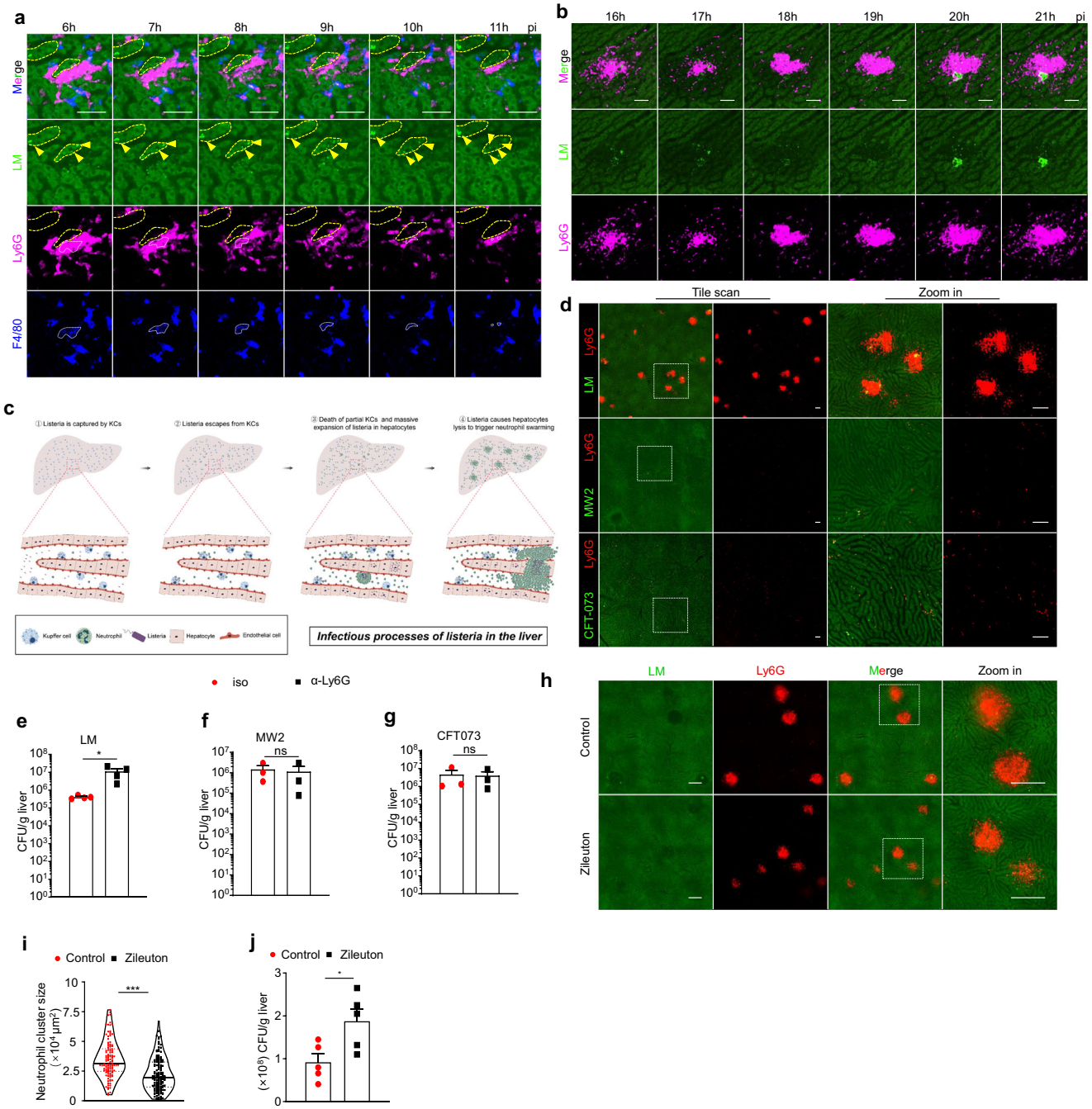

Fig. 2 | Neutrophil swarming is indispensable for controlling the early spread of LM. a Dynamic intravital images showing the distribution of LM and the behavior of neutrophils in the liver 6 h post-infection. Mice were infected with 1×10^8 CFU LM-GFP intravenously. APC anti-F4/80-labeled KCs (blue), PE anti-Ly6G-labeled neutrophils (purple), and LM-GFP (green) are shown. Yellow arrows indicate LM within hepatocytes. Yellow dashed lines indicate infected hepatocytes. White dashed lines indicate debris of KC. Scale bar, 50 μm. The experiment was repeated three times. **b** Dynamic intravital images showing the localization of LM and the behavior of neutrophils in the liver 16 h post-infection. Mice were infected with 1×10^6 CFU LM-GFP intravenously. PE anti-Ly6G-labeled neutrophils (purple) and LM-GFP (green) are shown. Scale bar, 50 μm. The experiment was repeated three times. **c** Depiction of the LM infection process in the liver during the initial 24 h. **d** Representative intravital images showing the distribution of neutrophils in the liver 24 h post-infection with 1×10^6 CFU LM-GFP, 5×10^7 CFU MW2-GFP, or 5×10^7 CFU CFT-073-GFP. Scale bar, 100 μm. The experiment was repeated twice. **e**–**g** Mice were treated with either iso or α-Ly6G 12 h prior to infections. Bacteria load in the liver was assessed at **e** 48 h post-infection with 1×10^6 CFU LM-GFP ($P = 0.0446$), 24 h post-infection with **f** 5×10^7 CFU MW2-GFP or **g** 5×10^7 CFU CFT-073-GFP. Each dot represents a mouse. Data were from 3 to 4 mice in each group. **h**–**j** Mice were treated with vehicle control or Zileuton (50 mg/kg). **h** Representative intravital images showing neutrophil cluster size in the liver 24 h post-infection with 1×10^6 CFU LM-GFP. Scale bar, 200 μm. **i** Quantification of neutrophil cluster size, with each dot representing an infection focus. Data were from three mice in each group. ($P < 0.0001$). **j** Bacterial load in the liver was assessed at 48 h post-infection with 1×10^6 CFU LM-GFP. Data were from five mice in each group. ($P = 0.0253$). Data are represented as mean ± SEM. $^*P < 0.05$; $^{**}P < 0.01$; $^{***}P < 0.001$; ns no significance.

https://doi.org/10.1038/s41467-024-53060-4

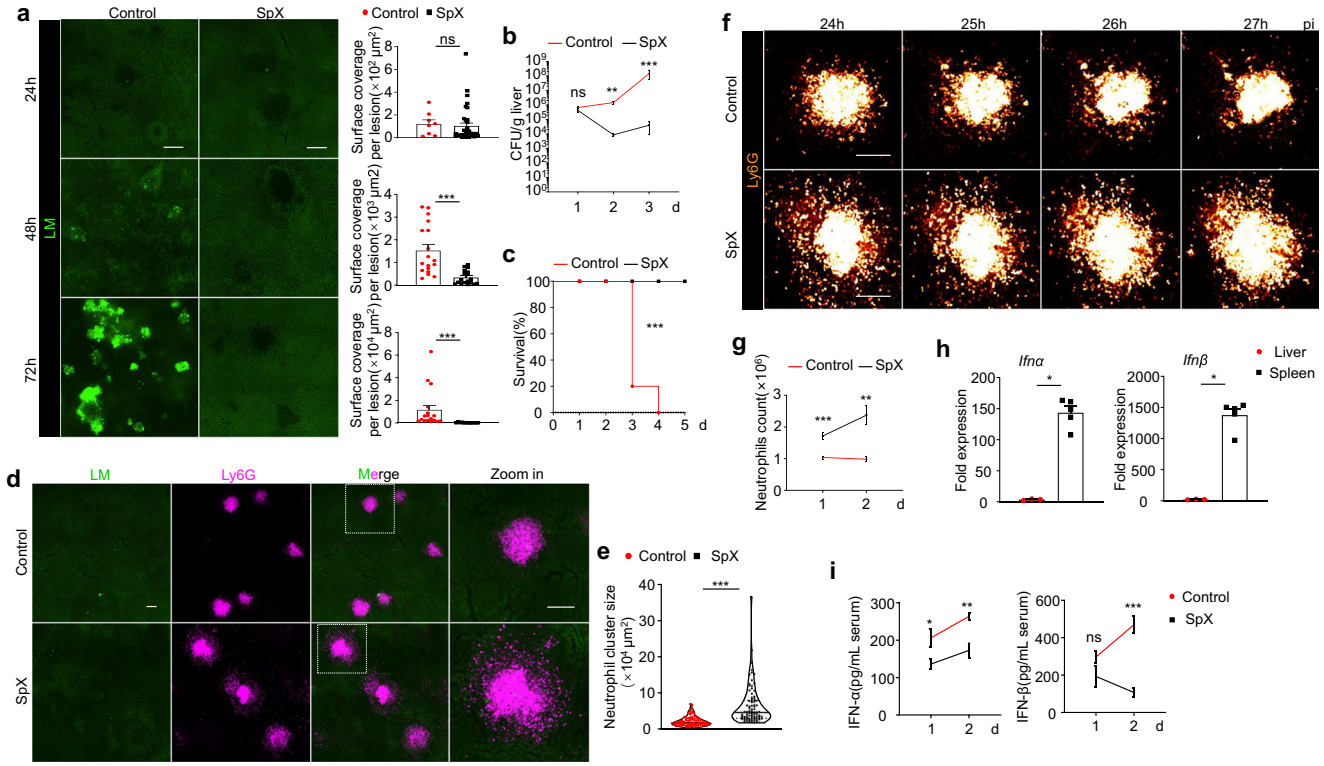

Fig. 3 | Increased resistance to LM infection in splenectomized mice is associated with enhanced neutrophil swarming. a–c Mice were subjected to sham surgery or underwent SpX. **a** Representative intravital images depicting the LM load in the liver at 24 h, 48 h ($P < 0.0001$), and 72 h ($P < 0.0001$) post-infection with 1×10^6 CFU LM-GFP. Scale bar, 200 μm. **b** Bacterial load in the liver was assessed at 24 h, 48 h ($P = 0.0079$), and 72 h ($P < 0.0001$) post-infection with 1×10^6 CFU LM-GFP. Data from the 24-h group were from ten mice in each group. Data for the 48 h group were from four mice in each group. Data for the 72 h group were from 9 (control) or 12 (SpX) mice. **c** The survival of mice infected with 1×10^6 CFU LM-GFP is shown. Data were from five mice in each group. ($P < 0.0001$). **d–g** Mice were subjected to sham surgery or underwent SpX. **d** Representative intravital images showing neutrophil clusters in the liver 24 h post-infection with 1×10^6 CFU LM-GFP. Scale bar, 100 μm. **e** Quantification of the size of neutrophil clusters, with each dot representing an infection focus. Data were from 3 to 5 mice in each group. ($P < 0.0001$). **f** Dynamic intravital images showing neutrophil swarming in the liver 24 h post-infection with 1×10^6 CFU LM-GFP. Scale bar, 100 μm. **g** Quantification of the number of neutrophils in the liver 24 h ($P = 0.0004$) and 48 h ($P = 0.0023$) post-infection with 1×10^6 CFU LM-GFP. Data were from five mice in each group. **h** Normalized mRNA levels of *Ifn-α* ($P = 0.0357$) and *Ifn-β* ($P = 0.0357$) in the liver and spleen at 24 h post-infection with 1×10^6 CFU LM-GFP. Data were from 3 to 5 mice in each group. **i** Quantification of serum levels of IFN-α ($P = 0.0369$; $P = 0.0031$) and IFN-β ($P = 0.0001$) at 24 h and 48 h post-infection with 1×10^6 CFU LM-GFP. Data were from five mice in each group. Data are represented as mean ± SEM. $^*P < 0.05$; $^{**}P < 0.01$; $^{***}P < 0.001$; ns no significance.

diminished the size of the injury but also led to unrestricted growth of LM in these regions (Supplementary Fig. 3c, d). Therefore, neutrophil swarming may contribute to LM control by disrupting the cellular microenvironment supporting bacterial replication, albeit at the cost of aggravated collateral tissue damage.

Increased resistance to LM infection in splenectomized mice is associated with enhanced neutrophil swarming

Although neutrophil swarming limited LM infection, all mice still died of uncontrollable bacterial growth 3–4 days after infection (Fig. 3a–c), suggesting that they were unable to halt the progression of LM infection. Previous studies have shown that splenectomized (SpX) mice exhibited increased resistance to LM infection[31]. Consistently, we observed improved survival and bacterial control in SpX mice compared to WT mice during LM infection (Fig. 3a–c). This has been attributed to the increased capacity of macrophages in LM clearance[32]. However, we observed that the difference in bacterial clearance became apparent 24 h after infection (Fig. 3b), a time point when LM had already evaded KCs, rendering them ineffective in eliminating LM. Even though we depleted KCs using clodronate liposomes, SpX mice still demonstrated better clearance of LM than sham control mice (Supplementary Fig. 4a, b). Instead, our results indicate that neutrophil responses were closely associated with the enhanced control of LM in SpX mice. At 6 h after infection, neutrophil numbers were comparable in SpX and WT mice, suggesting that the ability of neutrophils to migrate from the periphery into tissues remained intact (Supplementary Fig. 4c, d). However, neutrophil clusters in the liver of SpX mice were larger than those in the control group at 24 h post-infection (Fig. 3d, e). At this time, neutrophil swarming in the WT mice was already halted. In contrast, neutrophils in SpX mice continued to swarm towards the infection foci, resulting in further enlargement of the neutrophil clusters and an increase in hepatic infiltration of neutrophils (Fig. 3f, g and Movie S4). The intensified neutrophil swarming response was accompanied by visible necrotic areas in the liver, along with elevated serum levels of alanine transaminase (ALT) and aspartate transaminase (AST) in LM-infected SpX mice (Supplementary Fig. 4e–g), further supporting the notion that collateral liver damage caused by neutrophil swarming may contribute to the control of LM infection. Monocytes are critical for the protection against LM infection[33] and have been implicated in the termination of neutrophil swarming responses[26]. However, CCR2$^{RFP/+}$ monocytes were recruited similarly to the periphery of neutrophil clusters in both sham and SpX-treated mice (Supplementary Fig. 5a). In monocytopenic *Ccr2*$^{-/-}$ mice, the sizes of neutrophil swarms were comparable to those in WT mice, regardless of the presence or absence of the spleen (Supplementary Fig. 5b, c). These findings rule out the contribution of monocytes to the enhanced neutrophil swarming in SpX mice. In conclusion, these results suggest that efficient clearance of LM infection is associated

with prolonged and amplified neutrophil swarming responses, and limiting neutrophil swarming may represent a strategy allowing the immune escape of LM.

IFN-I aggravates LM infection by directly inhibiting neutrophil swarming

Despite the heightened neutrophil responses during LM infection, splenectomy did not alter the homeostatic properties of neutrophils. The cell number and maturity of circulating neutrophils remained unchanged in SpX mice at a steady state (Supplementary Fig. 4h), implying that the impact of LM on the spleen may underlie the regulation of neutrophil swarming. It has been reported that LM induces IFN-I production in the spleen, which is believed to impair the antibacterial function of macrophages, leading to the exacerbation of LM infection[34,35]. However, whether and how LM-induced IFN-I affects neutrophil function remains unclear. During early LM infection, approximately 5% of LM was sequestered in the spleen (Fig. 1a), and dynamic imaging revealed its rapid capture by red pulp macrophages (Supplementary Fig. 6a, b). Despite LM being predominantly captured by the liver rather than the spleen, the level of IFN-I expression was significantly higher in the spleen than in the liver (Fig. 3h). Moreover, serum levels of IFN-I were significantly lower in SpX mice than in sham control mice (Fig. 3i). These results led to the hypothesis that IFN-I may be the spleen-derived factor inhibiting neutrophil swarming. To this end, we utilized hydrodynamic injection (HDI) to induce sustained expression of IFN-I in the liver[36]. As expected, overexpression of IFN-I reduced the size of neutrophil clusters induced by LM, regardless of sex (Fig. 4a, b and Supplementary Fig. 6c), resulting in exacerbated LM infection (Fig. 4c). Similarly, augmented neutrophil swarming in SpX mice was severely blunted upon IFN-I overexpression (Supplementary Fig. 6d). Most importantly, type I IFN receptor (IFNAR) deficiency led to enhanced neutrophil swarming during LM infection in control mice, but not in SpX mice (Fig. 4d–f).

Based on these findings, we infer that LM-stimulated splenic production of IFN-I may act on circulating neutrophils to impair their intrinsic ability to swarm within tissues. Supporting this, the inhibitory effect of IFN-I on neutrophil swarming was also evident in the infected spleen (Supplementary Fig. 6e–h). Furthermore, we established a Bacterial AGAR pellet imaging system (Fig. 4g), where neutrophils were attracted to and penetrated LM-encapsulated agar pellets, exhibiting a typical swarming behavior that was dependent on LM-triggered LTB4 production in neutrophils and thus could be antagonized by Zileuton (Supplementary Fig. 7a–d and Movie S5). In this model, IFN-I stimulation significantly suppressed neutrophil swarming (Fig. 4h, i and Movie S5). In addition, blood neutrophils isolated from SpX mice that had impaired IFN-I production exhibited enhanced swarming responses compared to those from sham-treated mice (Supplementary Fig. 7e, f). Notably, IFN-I treatment of isolated neutrophils had negligible effects on their phagocytosis, ROS production, and killing of LM in vitro (Supplementary Fig. 7g–i), suggesting a minimal impact of IFN-I on the bactericidal function of neutrophils. Collectively, these results indicate that IFN-I can directly regulate neutrophil function mainly through inhibiting swarming responses, thereby exacerbating LM infection.

IFN-I inhibits neutrophil swarming by antagonizing the activation of the ERK signaling pathway

Neutrophil swarming largely relies on the autocrine activity of LTB4[8]. IFN-I stimulation inhibited 5-LOX expression and LTB4 synthesis in isolated neutrophils, providing mechanistic insights into the impaired neutrophil swarming (Supplementary Fig. 8a–e). A previous study highlighted the existence of an LTB4/ERK/5-LOX/LTB4 positive feedback signaling axis, which closely resembles the feed-forward mechanism of neutrophil swarming[37]. Additionally, it has been reported that IFN-I can inhibit the activation of ERK[38]. Therefore, we wondered whether IFN-I affected LTB4 production and the swarming of neutrophils through the ERK pathway. Indeed, the phosphorylation of ERK in neutrophils was induced by LTB4 treatment, but was inhibited in the presence of IFN-I (Fig. 5a–d). Furthermore, the p-ERK inhibitor PD0325901 decreased LTB4 synthesis in neutrophils (Supplementary Fig. 8e), and suppressed their swarming towards bacterial agar pellets (Fig. 5e, f and Movie S5). Consistently, in vivo administration of PD0325901 also significantly decreased neutrophil clusters induced by LM (Fig. 5g, h), while exacerbating LM infection (Fig. 5i). Since binding of IFN-I to IFNAR primarily activates the JAK-STAT pathway[39], we aimed to investigate whether IFN-I inhibits ERK signaling in a JAK-STAT-dependent manner. As expected, the JAK1/2 inhibitor Ruxolitinib rescued LTB4-induced ERK phosphorylation in the presence of IFN-I (Fig. 5j, k), and largely abolished IFN-I-mediated suppression of neutrophil swarming in vitro (Fig. 5l, m). Since integrins are also essential for neutrophil swarming and CD11b upregulation is pivotal for neutrophil migration[8,40], we investigated whether IFN-I affects CD11b expression in neutrophils. Our results showed that neutrophils in LM-infected WT and *Ifnar*$^{-/-}$ mice had comparable levels of CD11b expression (Supplementary Fig. 8f), and IFN-I stimulation in vitro even slightly increased CD11b expression on neutrophils (Supplementary Fig. 8g). These data exclude the possibility that IFN-I suppresses neutrophil swarming by inhibiting CD11b expression. Taken together, these results suggest that IFNAR-JAK signaling disrupts the forward loop of neutrophil swarming by antagonizing LTB4-mediated activation of the ERK pathway, effectively preventing further amplification of the signaling cascade.

Virus-induced IFN-I aggravates secondary LM infection by inhibiting neutrophil-swarming

Viral infections are well known to induce upregulation of IFN-I levels. Therefore, we wonder whether neutrophil swarming is inhibited during co-infections with viruses and bacteria, potentially exacerbating secondary bacterial infections. To establish a coinfection model, we pre-infected mice with either vesicular stomatitis virus (VSV, an RNA virus) or murine cytomegalovirus (MCMV, a DNA virus), and subsequently evaluated their susceptibility to secondary LM infection (Fig. 6a). In line with our speculation, both VSV and MCMV were able to enhance secondary LM infection, leading to increased bacterial burden in the liver of virally co-infected mice (Fig. 6b, c), which could be attributed to the decrease in the formation of neutrophil clusters during secondary LM infection (Fig. 6d–g). Previous reports have indicated that influenza virus infection can also exacerbate secondary LM infection[41]. Consistently, our results revealed a significant reduction in the formation of neutrophil clusters induced by LM upon influenza virus infection (Supplementary Fig. 9a–c).

To assess the impact of viral infection on neutrophil dynamics, we examined the proportion and migration of neutrophils in the co-infection model. Viral infection did not affect the proportion or number of neutrophils in the bone marrow after secondary LM infection (Supplementary Fig. 9d, e). Additionally, the liver infiltration of neutrophils was comparable between co-infected mice and mice infected with LM alone at both 6 h (Supplementary Fig. 9f, g) and 24 h (Supplementary Fig. 9h, i) after LM infection. Consistently, intravital imaging of the cremaster muscle demonstrated normal neutrophil transendothelial migration, unaffected by viral infection (Supplementary Fig.9j–l and Movie S6). These results suggest that preexisting viral infection does not directly affect neutrophil numbers or tissue infiltration.

However, at 16 h post-LM infection, the neutrophil clusters were much smaller in co-infected mice compared to those with LM infection alone (Fig. 6h, i and Movie S7), suggesting that a preexisting viral infection suppresses neutrophil swarming induced by subsequent LM infection. Additionally, viral infection was aggravated in *Ifnar*$^{-/-}$ mice, but the size of neutrophil clusters induced by LM was enlarged as compared to that in WT mice (Fig. 6j, k). To exclude the effects of

https://doi.org/10.1038/s41467-024-53060-4

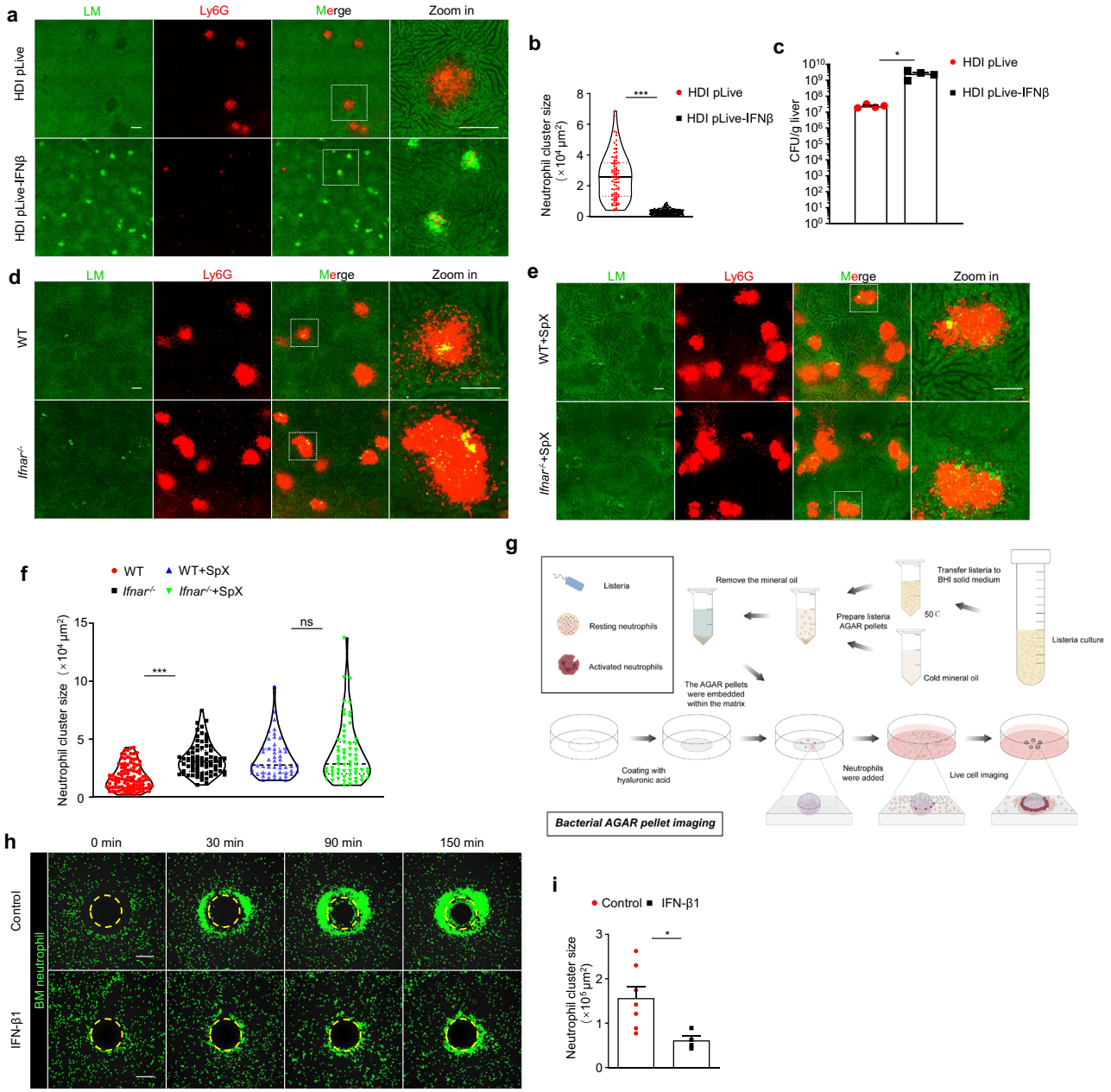

Fig. 4 | IFN-I aggravates LM infection by directly inhibiting neutrophil swarming. a–**c** Mice were subjected to HDI with 5 μg pLive or pLive-*IFNβ* plasmid 5d prior to infection. **a** Representative intravital images showing neutrophil clusters in the liver 24 h post-infection with 1×10^6 CFU LM-GFP. Scale bar, 200 μm. **b** Quantification of the size of neutrophil clusters, with each dot representing an infection focus. Data were from three mice in each group. ($P < 0.0001$). **c** Bacterial load in the liver was assessed at 48 h post-infection with 1×10^6 CFU LM-GFP. Data were from four mice in each group. ($P = 0.0268$). **d** WT and *Ifnar*$^{-/-}$ mice were infected with 1×10^6 CFU LM-GFP. Representative intravital images showing neutrophil clusters in the liver at 24 h post-infection with 1×10^6 CFU LM-GFP. Scale bar, 100 μm. **e** WT and *Ifnar*$^{-/-}$ mice underwent SpX. Representative intravital images showing neutrophil clusters in the liver at 24 h post-infection with 1×10^6 CFU LM-GFP. Scale bar, 100 μm. **f** Quantification of the size of neutrophil clusters, with each dot representing an infection focus. Data were from three mice in each group. ($P < 0.0001$). **g** Illustration of the procedure for bacteria AGAR pellet imaging. **h** Bacteria AGAR pellet imaging was conducted to visualize neutrophil swarming with and without IFN-β1 treatment. Scale bar, 200 μm. **i** Quantification of neutrophil cluster size at 150 min post-imaging, with each dot representing a neutrophil cluster. The experiment was repeated twice and statistically analyzed. ($P = 0.0284$). Data are represented as mean ± SEM. *$P < 0.05$; **$P < 0.01$; ***$P < 0.001$.

aggravated viral infections in *Ifnar*$^{-/-}$ mice, we purified neutrophils from the bone marrow of both WT and *Ifnar*$^{-/-}$ mice, mixed them in a 1:1 ratio, and transferred them into WT mice for co-infection. The adoptive transfer of mixed neutrophils had no impact on the progression of viral or LM infections (Supplementary Fig. 9m–o). However, the proportion of *Ifnar*$^{-/-}$ neutrophils in the infected foci was much higher than that of WT neutrophils (Fig. 6l), suggesting a cell-intrinsic effect of type I IFN signaling in suppressing neutrophil swarming. In conclusion, these results indicate that virus-induced IFN-I can promote secondary bacterial infections by inhibiting neutrophil swarming at the local tissue level.

IFN-I inhibits human neutrophil swarming by deactivating the ERK pathway

To investigate whether IFN-I also regulates the swarming behavior of human neutrophils during co-infection, we induced human HL-60 cells to differentiate into neutrophil-like cells, known as dHL-60 cells, using DMSO[42]. Similar to mouse bone marrow neutrophils, the swarming of

https://doi.org/10.1038/s41467-024-53060-4

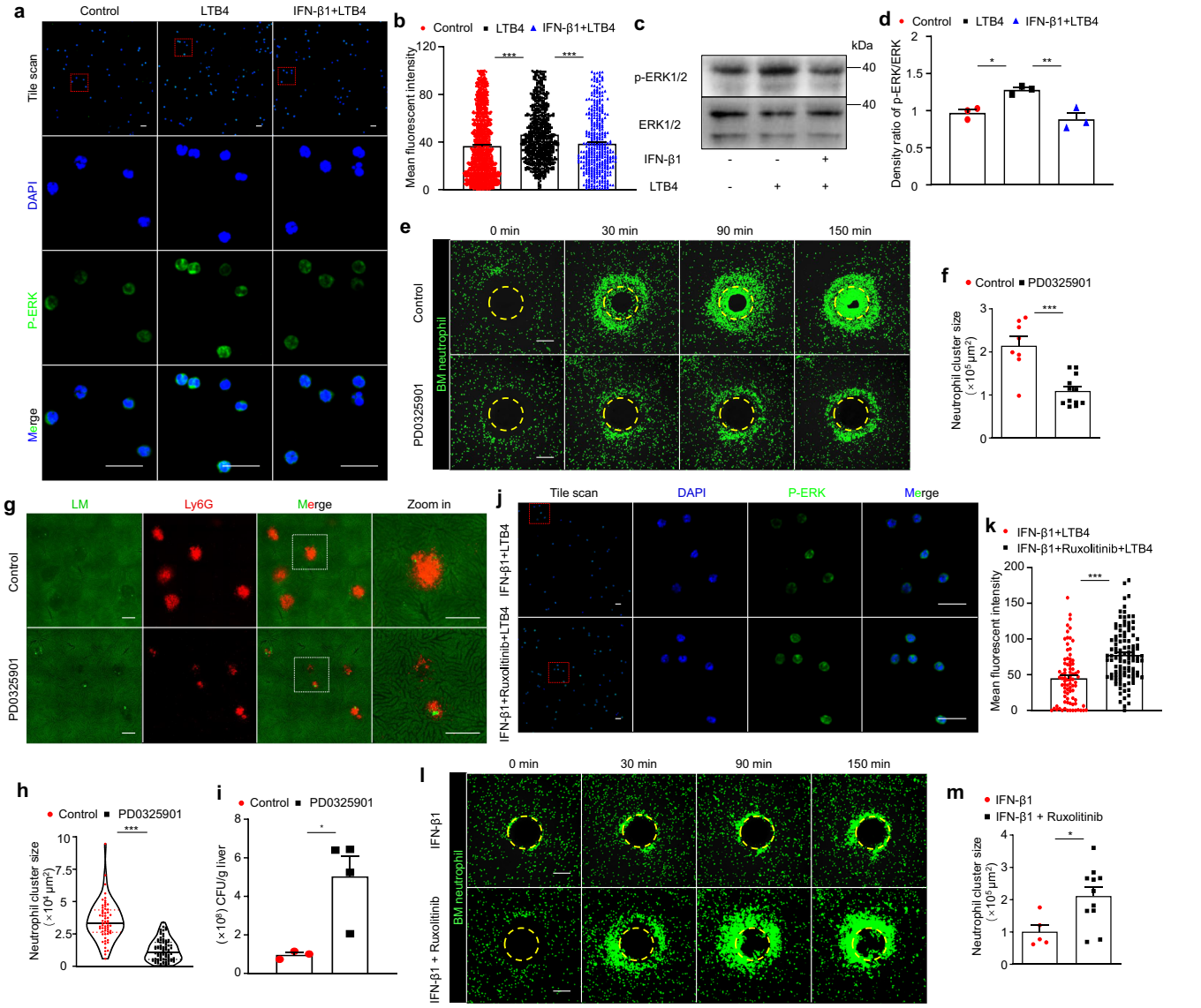

Fig. 5 | IFN-I inhibits neutrophil swarming by antagonizing the activation of the ERK signaling pathway. a, **b** Bone marrow neutrophils were treated with IFN-β1 and LTB4. Representative immunofluorescent images (**a**) and statistics (**b**) of p-ERK in neutrophils with indicated treatment are shown. Each dot represents one cell. The experiment was repeated three times and statistically analyzed. Scale bar, 20 μm. ($P < 0.0001$; $P < 0.0001$). **c**, **d** Immunoblot analysis was performed to assess the level of p-ERK in neutrophils with and without IFN-β1 treatment. The experiment was repeated three times and statistically analyzed. ($P = 0.0196$; $P = 0.0062$). **e** Bacteria AGAR pellet imaging was conducted to compare BM neutrophil swarming between samples treated with and without PD0325901 (5 μg/mL) for 4 h prior to imaging. Scale bar, 200 μm. **f** Quantification of neutrophil cluster size at 150 min post-imaging, with each dot representing a neutrophil cluster. The experiment was repeated twice and statistically analyzed. ($P < 0.0001$). **g**–**i** Mice were treated with vehicle or PD0325901 (40 mg/kg). **g** Representative intravital images showing neutrophil clusters in the liver 24 h post-infection with 1×10^6 CFU LM-GFP. Scale bar, 200 μm. **h** Quantification of the size of neutrophil clusters, with each dot representing an infection focus. Data are from three mice in each group. ($P < 0.0001$). **i** Bacterial load in the liver was assessed at 48 h post-infection with 1×10^6 CFU LM-GFP. Data are from 3 to 4 mice in each group. ($P = 0.0208$). **j**, **k** Bone marrow neutrophils were treated with IFN-β1 plus LTB4 in the presence or absence of Ruxolitinib (20 μg/mL). Representative immunofluorescent images (**j**) and statistics (**k**) of p-ERK in neutrophils with indicated treatment are shown. Each dot represents one cell. The experiment was repeated twice and statistically analyzed. Scale bar, 20 μm. ($P < 0.0001$). **l** Bacteria AGAR pellet imaging was conducted to visualize neutrophil swarming with and without Ruxolitinib in the presence of IFN-β1 stimulation. Scale bar, 200 μm. **m** Quantification of neutrophil cluster size at 150 min post-imaging, with each dot representing a neutrophil cluster. The experiment was repeated twice and statistically analyzed. ($P = 0.0221$). Data are represented as mean ± SEM. *$P < 0.05$; ***$P < 0.001$.

dHL-60 cells could also be induced by LM-encapsulated bacterial agar pellets and be inhibited by Zileuton (Supplementary Fig. 10a, b, and Movie S8). As expected, IFN-I treatment also inhibited dHL-60 cell swarming (Fig. 7a, b and Movie S8). In addition, IFN-I treatment suppressed the phosphorylation of ERK and inhibited the expression of 5-LOX in dHL-60 cells (Fig. 7c–f). Similarly, PD0325901 treatment reduced the responsiveness of dHL-60 cells to bacterial agar pellets (Fig. 7g, h and Movie S8). Considering that secondary bacterial infections are a significant cause of mortality in COVID-19 patients[43], we collected peripheral blood samples from individuals diagnosed with COVID-19 and isolated their neutrophils. Consistent with previous reports[44], serum IFN-I levels were significantly elevated in these patients (Fig. 7i). The neutrophil swarming of COVID-19 patients was weaker than that of their healthy counterparts (Fig. 7j, k and Movie S9). In addition, the phosphorylation of ERK and the expression of *ALOX5* in these neutrophils were also reduced (Supplementary Fig. 10c, e). In summary, these results suggest that the inhibitory mechanism of IFN-I on neutrophil swarming is applicable to human neutrophils.

https://doi.org/10.1038/s41467-024-53060-4

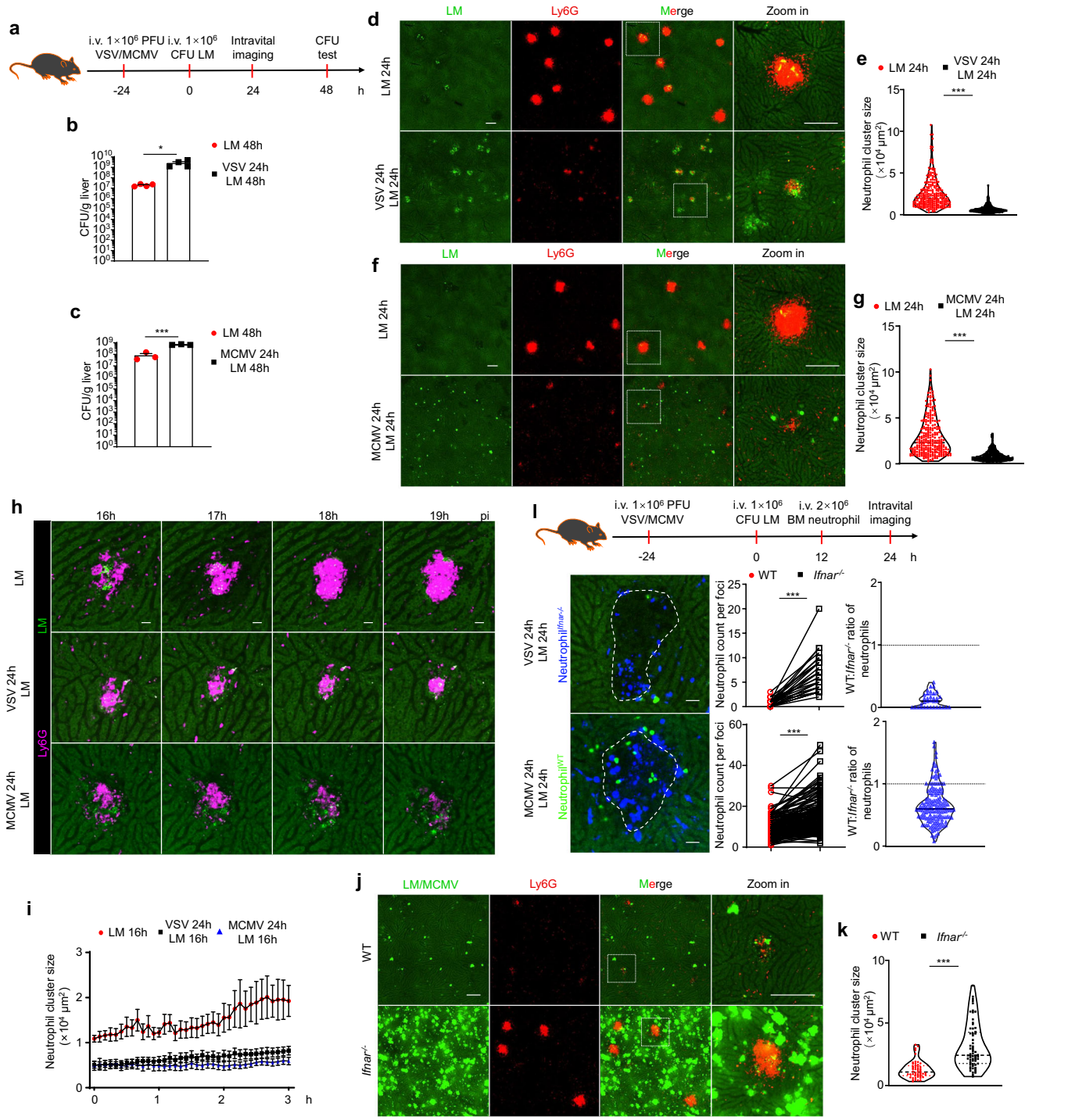

Fig. 6 | Virus-induced IFN-I aggravates secondary LM infection by inhibiting neutrophil swarming. a–**c** Mice were infected with 1×10^6 PFU **b** VSV ($P = 0.0286$) or **c** MCMV (P = 0.0002) 24 h prior to LM infection, and bacterial load in the liver was assessed at 48 h post-infection with 1×10^6 CFU LM-GFP. Data are from 3 to 4 mice in each group. **d**–**g** Mice were infected with 1×10^6 PFU **d** VSV or **f** MCMV 24 h prior to LM-GFP infection, and representative intravital images showing neutrophil clusters in the liver 24 h post-infection with 1×10^6 CFU LM-GFP. Scale bar, 200 μm. **e**, **g** Quantification of the size of neutrophil clusters, with each dot representing an infection focus. Data were from 3 to 5 mice in each group. ($P < 0.0001$; $P < 0.0001$). **h** Mice were infected with vehicle control, 1×10^6 PFU VSV or MCMV 24 h prior to with LM-GFP infection, and dynamic intravital images showing the neutrophil swarming in the liver 16 h post-infection with 1×10^6 CFU LM-GFP. Scale bar, 50 μm. **i** Quantification of neutrophil cluster sizes at 5-min intervals. Data of the LM group were from three mice. Data of the VSV + LM group were from five mice. Data from the MCMV + LM group were from three mice. **j** WT and *Ifnar*$^{-/-}$ mice were infected with 1×10^6 PFU MCMV 24 h prior to LM infection, and representative intravital images showed neutrophil clusters in the liver 24 h post-infection with 1×10^6 CFU LM-GFP. Scale bar, 200 μm. **k** Quantification of the size of neutrophil clusters, with each dot representing an infected focus. Data were from three mice in each group. ($P < 0.0001$). **l** Mice were infected with 1×10^6 PFU VSV or MCMV 24 h before LM infection. 1×10^6 WT and 1×10^6 *Ifnar*$^{-/-}$ neutrophils were co-transferred 12 h after LM infection. Quantification of the number of donor neutrophils within foci, with each dot representing an infection focus. Scale bar, 50 μm. Data were from three mice in each group. ($P < 0.0001$; $P < 0.0001$). Data are represented as mean ± SEM. *$P < 0.05$; ***$P < 0.001$.

https://doi.org/10.1038/s41467-024-53060-4

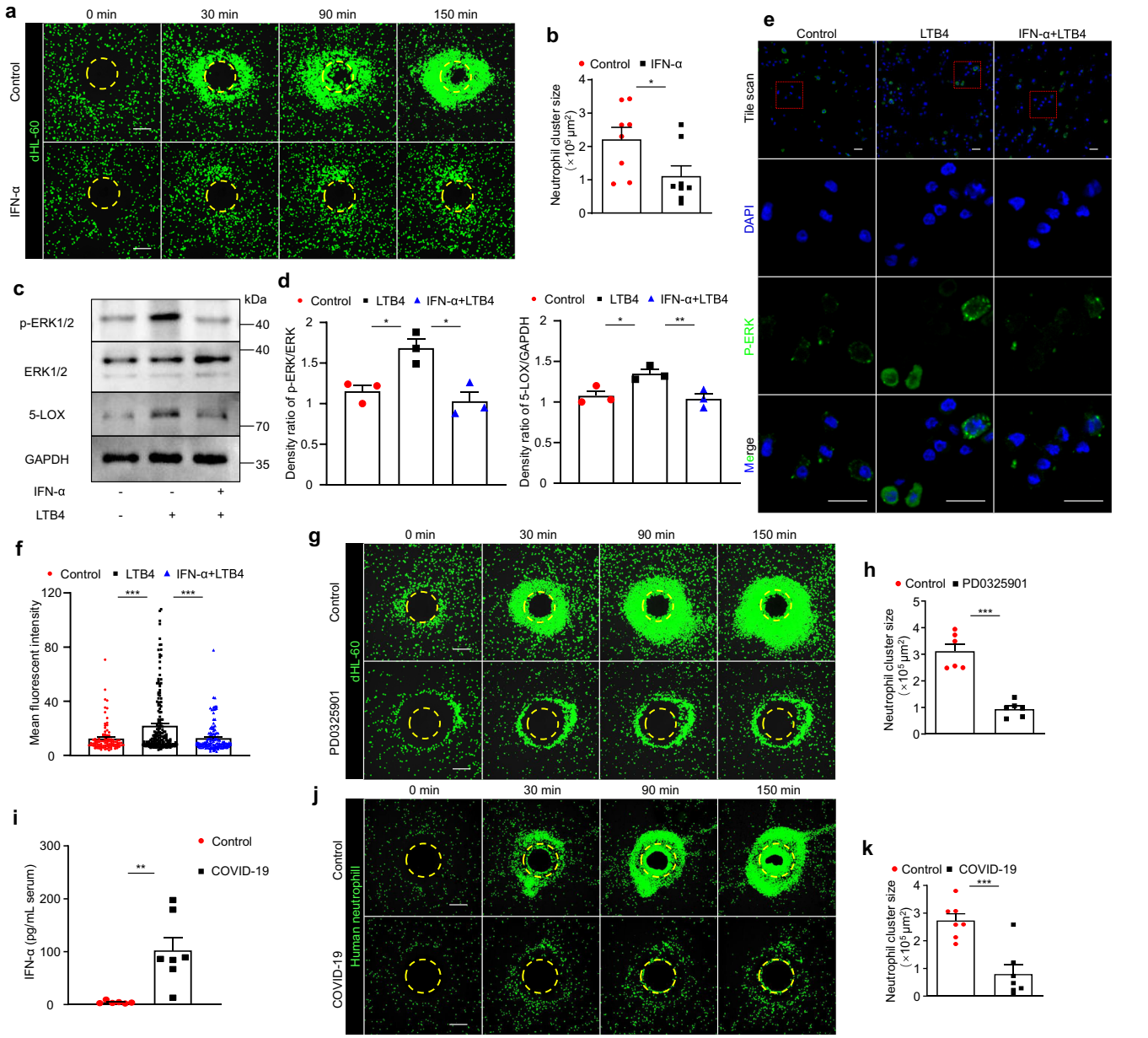

Fig. 7 | IFN-I inhibits human neutrophil swarming by deactivating the ERK pathway. a Bacteria AGAR pellet imaging was conducted to compare the swarming of dHL-60 cells with and without IFN-α (100 ng/mL) treatment. Scale bar, 200 μm. **b** Quantification of neutrophil cluster size at 150 min post-imaging, with each dot representing a neutrophil cluster. The experiment was repeated twice and statistically analyzed. ($P = 0.0354$). **c**, **d** dHL-60 cells were treated with IFN-α and LTB4. Immunoblot analysis of p-ERK ($P = 0.0259$; $P = 0.0102$) and 5-LOX ($P = 0.0396$; $P = 0.0236$) in dHL-60 cells was conducted. The experiment was repeated three times and statistically analyzed. **e**, **f** Representative immunofluorescent images (**e**) and statistics (**f**) of p-ERK in dHL-60 cells with indicated treatment are shown. Each dot represents one cell. The experiment was repeated twice and statistically analyzed. Scale bar, 20 μm. ($P < 0.0001$; $P < 0.0001$). **g** Bacteria AGAR pellet imaging was conducted to compare dHL-60 neutrophil swarming between samples with and without PD0325901 (5 μg/mL) treatment. Scale bar, 200 μm. **h** Quantification of neutrophil cluster size at 150 min post-imaging, with each dot representing a neutrophil cluster. The experiment was repeated twice and statistically analyzed. ($P < 0.0001$). **i** Quantification of serum levels of IFN-α in healthy controls and COVID-19 patients, with each dot representing one person. The experiment was repeated twice and statistically analyzed. ($P = 0.0012$). **j** Bacterial agar pellet imaging was performed to compare the swarming behavior of human peripheral blood neutrophils between healthy controls and COVID-19 patients. Scale bar, 200 μm. **k** Quantification of neutrophil cluster size at 150 min post-imaging, with each dot representing one person. The experiment was repeated four times and statistically analyzed. ($P = 0.0005$). Data are represented as mean ± SEM. $^{*}P < 0.05$; $^{**}P < 0.01$; $^{***}P < 0.001$.

Discussion

In this study, we observed that LM rapidly escaped from KCs and replicated within hepatocytes rather than within KCs. Due to macrophages serving as the primary host for LM, extensive studies have focused on investigating the mechanisms of interaction between LM and macrophages at the cellular level[2]. However, it is important to acknowledge that these mechanisms only operate when LM remains within the confines of the macrophage. Once LM escapes from the macrophage, these mechanisms become ineffective. In fact, the unique escape mechanisms employed by LM render in vivo infections more intricate than their in vitro counterparts at the cellular level. In our study, we found that LM is capable of prompt evasion from KCs in an LLO-dependent manner, as early as 2–3 h post-infection. The ActA-mediated cell-to-cell spread, appears to be nonessential for LM to

escape from KCs and for their clearance in the liver. Nevertheless, there exists literature suggesting that ActA plays a crucial role in LM invasion of the nervous system[45], indicating that LM employs different invasion strategies in distinct tissues.

Macrophages play a crucial role in host defense against bacterial infections due to their potent bactericidal capacity. However, they suffer from a critical limitation—poor mobility. In contrast, neutrophils compensate for this weakness with their remarkable ability to move freely, enabling them to traverse the body and effectively address the limitations of macrophages. Despite their significant infiltration into the liver following LM infection, there exists conflicting evidence regarding the involvement of neutrophils in controlling LM infection[6,46]. We hypothesize that these discordant results may be attributed to the differential timing of neutrophil clearance mediated by antibodies. In the past, it was widely believed that neutrophils could exert their function once they infiltrated the local tissue[47]. However, it is now recognized that upon infiltration into the tissue, neutrophils undergo further activation to congregate in damaged foci[8]. Our results demonstrate that once neutrophil clusters form, antibodies are unable to label neutrophils within the clusters (unpublished data). Consequently, using antibodies to clear neutrophils after LM infection may lead to ineffective neutrophil clearance. Conversely, clearing neutrophils using antibodies before LM infection significantly exacerbates LM infection, highlighting the role of neutrophils in controlling LM infection. In fact, we showed that aggregated neutrophils can actively take up and eliminate extracellular LM, as well as induce bystander death of hepatocytes, thereby forming an immune barrier to limit LM invasion.

However, neutrophils also have limitations. On one hand, our imaging results revealed that once LM escapes from KCs, it quickly infects hepatocytes. Although neutrophils have already infiltrated the liver at this stage, they fail to locate LM hiding within hepatocytes, leading to significant propagation of LM within these cells. On the other hand, we observed that despite hepatocyte lysis releasing LM and triggering neutrophil activation, LM can employ additional mechanisms such as IFN-I to inhibit neutrophil function. IFN-I has been implicated as a potent regulator for many aspects of neutrophil activity, such as their lifespan[48], chemotaxis[19,49], and cytokine production[50]. Our findings revealed a cell-intrinsic effect of IFN-I in suppressing neutrophil swarming without compromising their bactericidal capacity or transendothelial migration during LM infection. This further highlights the complexity of context-dependent IFN-I signaling in modulating innate immune responses. In fact, neutrophils are not the only innate immune cell type affected by IFNAR signaling, LM-triggered IFN-I production is also reported to be detrimental to the antimicrobial activity of macrophages by inhibiting their activation and sensitizing them to death[51]. Given that monocytes entered the infection foci in large quantities almost simultaneously with neutrophils, IFN-I may be exploited by LM to evade immune surveillance from monocytes and/or their macrophage derivatives.

Despite the critical role of IFN-I in promoting innate immune evasion of LM in the liver, our results indicate that IFN-I is predominately produced in the spleen. Consequently, splenectomy abolished IFN-I production, resulting in enhanced neutrophil swarming and improved LM control. These data pinpoint a spleen-liver axis in regulating anti-microbial defense. Indeed, various splenic cell types, including macrophages, pDCs, Tip-DCs, and even B cells, are reported to produce IFN-I upon LM infection[52], possibly due to the rapid shuttling of LM within different host cells in the spleen[53]. These cells may collectively contribute to elevated IFN-I levels in the circulation, which systemically impact the ability of neutrophils to swarm by antagonizing their intracellular ERK signaling in an IFNAR-JAK-dependent manner. In support of this, blood neutrophils that had not experienced robust IFN-I stimulation, such as those isolated from SpX-treated mice, exhibited intact swarming behavior. Conversely, blood neutrophils from COVID-19 patients with elevated serum levels of IFN-I displayed impaired swarming.

Viral infections typically result in an increase in IFN-I levels, which can control viral infections through various mechanisms and have been reported to inhibit the recruitment of neutrophils during viral infections[49]. The role of neutrophils in controlling viral infections remains not fully understood and is subject to debate. While there are reports suggesting that neutrophils can release NETs to inhibit viral spread[54], there are also instances where neutrophils can act as viral carriers, contributing to viral dissemination[55]. However, frequent reports of severe immunopathology resulting from neutrophil infiltration at the site of viral infection indicate that the organism must make cautious decisions regarding the utilization of neutrophils. Interestingly, we found that enhanced neutrophil swarming in SpX mice was correlated with severe liver damage. Intracellular bacteria such as LM and *M. tuberculosis* share similarities with viruses, for example, their ability to activate IFN-I expression[56,57]. We observed that IFN-I can restrict neutrophil swarming to prevent excessive tissue damage, and LM might exploit this mechanism to evade immune surveillance by neutrophils. Notably, viral infections in clinical settings often lead to secondary bacterial infections, independent of the specific types of viruses and bacteria involved[58,59]. Our results indicate that different viruses can exacerbate secondary LM infections through the virus-induced production of IFN-I, which inhibits neutrophil swarming. Of note, viral infection did not affect neutrophil rolling, tethering, or transmigration in inflamed vessels. This somewhat supports the notion that IFN-I does not impair integrin activation, which is essential for neutrophil mobility. Although the precise molecular mechanisms by which IFN-I uncouples neutrophil transendothelial migration from swarming remain to be elucidated, abrogation of the LTB4-mediated feedback loop is at least partially involved. Nevertheless, our results highlight the function of IFN-I in ensuring an appropriate neutrophil response during viral infection, thereby preventing excessive tissue damage, albeit at the cost of increased sensitivity to secondary bacterial infections. These findings underscore the importance of prophylactic use of antibiotics as adjunctive therapy in clinical settings for patients with severe viral infections, particularly those who require exogenous IFN-I treatment.

In conclusion, our study utilized liver intravital imaging to provide a comprehensive and detailed understanding of the dynamic process of LM infection in the liver. We have identified that LM employs distinct immune evasion strategies that target different cellular characteristics. Exploiting the relatively low motility of KCs, LM employs LLO to puncture the cell membrane of KCs, facilitating its escape and avoiding KC-mediated elimination. To evade immune surveillance by neutrophils, LM strategically proliferates inside hepatocytes, reducing its exposure to neutrophil detection. Furthermore, it can induce IFN-I to evade neutrophil-mediated elimination. These findings underscore significant differences between in vivo and in vitro infection of the pathogen, highlighting the importance of studying pathogens within their natural microenvironment. Future studies aimed at elucidating the dynamic interactions between LM and other immune cells could allow us to gain deeper insights into the intricate co-evolutionary processes of pathogen-host competition. Such investigations will undoubtedly enhance our understanding of infectious diseases and facilitate the development of more effective strategies for combatting them.

Methods

Ethics statement

Animal experiments were conducted following the guidelines established by the Animal Care Committee of USTC (USTCACUC192401034). The use of human peripheral blood has been reviewed and approved by the Medical Research Ethics Committee of the First Affiliated Hospital of USTC (2023KY369), with informed consent obtained from all volunteers.

Mice

C57BL/six mice were purchased from Nanjing GemPharmatech Co., LTD. *Ly6g*-Cre-2A-tdTomato mice (Cat. NO. NM-KI-200219) were purchased from Shanghai Model Organisms Center, Inc. *Ifnar*$^{-/-}$ mice, mT/mG mice, and CCR2$^{RFP/RFP}$ ki/ko mice were originally from the Jackson Laboratory. *Padi4*$^{-/-}$ mice were originally from Cyagen Bioscience Inc. All mice were housed in specific pathogen-free (SPF) facilities at USTC. Unless otherwise specified, all mice used in the experiments were male, ranging in age from 6 to 12 weeks.

Antibodies and reagents

Fluorescein-conjugated antibodies, including APC/Cy7 anti-mouse CD45 (30-F11), PE/Cy7 anti-mouse CD11b (M1/70), PE or AF647 anti-mouse Ly6G (1A8), APC or PE anti-mouse F4/80 (BM8), AF647 anti-mouse CD31 (MEC13.3), APC anti-mouse CD169 (3D6.112), PE/Cyanine7 anti-mouse CD117 (c-kit) (2B8), Brilliant Violet 605™ anti-mouse CD184 (CXCR4) (L276F12), APC anti-mouse CD182 (CXCR2) (SA045E1), 488 anti-mouse CD170 (Siglec-F) (S17007L), and PerCP/Cy5.5 anti-mouse Ly-6C (HK1.4) were obtained from Biolegend and used for flow cytometry or intravital imaging. Brilliant Violet™ 786 anti-mouse CD11b (M1/70) was obtained from eBioscience and used for flow cytometry. The antibodies used for western blotting or immunofluorescence were as follows: GAPDH monoclonal antibody (abs830030, 1:2000, Absin); ERK1/2 polyclonal antibody (11257-1-AP, 1:1000, Proteintech); phospho-ERK1/2 (Thr202/Tyr204) polyclonal antibody (28733-1-AP, 1:1000 or 1:200, Proteintech) and 5-LOX polyclonal antibody (10021-1-Ig, 1:100, Proteintech). Three-color prestained protein Marker (EC1019) was from Shandong Sparkjade Biotechnology Co., Ltd. The BCA Protein Assay Kit (PA002-01A) was obtained from Novoprotein. The EndoFree Plasmid Midi Kit (CW2105S) was from obtained CWBIO. CFSE cell division tracker kit (5 μM, Cat. 423801) and PI (25 μg, Cat. 421301) were purchased from BioLegend. DiD (5 μM, Cat. D7757) was from Invitrogen. DCFH-DA (2′,7′-Dichlorofluorescin diacetate) (10 μM, Cat. D6883) was from Sigma. LTB4 (1 μM, Cat. 20110) was from Cayman. LPS (200 ng/mL, Cat. L2630) and fMLP (1 μM, Cat. F35065) were from Sigma. Recombinant mouse IFN-β1 (20 ng/mL, Cat. 581302) and recombinant human IFN-α (100 ng/mL, Cat. 592702) were from Biolegend. Zileuton (Cat. S1443), PD0325901 (Cat. S1036), Ruxolitinib (Cat. S1378), Cl-amidine (Cat. S8141), and Setanaxib (Cat. S7171) were from Selleck. Clodronate liposomes (100 μL, Cat. C44J0819) were from LIPOSOMA.

Cell lines and plasmids

The HL-60 cell line was obtained from Prof. Wen Pan (USTC) and was cultured in Roswell Park Memorial Institute (RPMI) 1640 medium supplemented with 10% FBS at 37 °C in a 5% CO_2 incubator. The pLive plasmid was kindly provided by Prof. Rui Sun (USTC). The DNA fragment encoding *ifnβ* was cloned and then inserted into the pLive plasmid for constructing the pLive-IFNβ plasmid. For HDI, mice were injected with 5 μg of pLive or pLive-IFNβ plasmid in 2 mL of saline within a duration of 8–10 s.

Viruses and bacteria

MCMV viral stocks were kindly provided by Prof. Zhigang Tian (USTC). VSV and IFV were kindly provided by Prof. Daxing Gao (USTC). Mice were intravenously infected with MCMV (1×10^6 PFU), VSV (1×10^6 PFU), or IFV (1×10^4 PFU). LM were kindly provided by Prof. Weihuan Fang (Zhejiang University). LM-GFP, LM-Δ*actA*-GFP and LM-Δ*hly*-GFP were kindly provided by Prof. Ning Wu (Huazhong University of Science and Technology). All LM strains were derived from the 10403S strain and were cultured in brain heart infusion (BHI) medium supplemented with 5 μg/mL erythromycin until reaching the logarithmic growth phase (OD600 nm = 0.5). Mice were intravenously infected with LM, using either 1×10^6 or 1×10^8 CFU. Additionally, subcutaneous infection was administered with 1×10^8 CFU. GFP-tagged MW2 was generated as described previously[60] and was cultured overnight in BHI medium supplemented with 5 μg/mL erythromycin, followed by subculture until the logarithmic phase (OD600 nm = 1.0). GFP-tagged *E. coli* was generated by electroporating the pSLC-284-vsfGFP plasmid into the CFT-073 strain and was cultured in LB medium supplemented with 50 μg/mL kanamycin until the logarithmic phase (OD600 nm = 0.6). Mice were intravenously infected with 5×10^7 CFU MW2 or CFT-073. To assess bacterial load in organs, tissue homogenates were diluted serially using PBS and then plated onto agar medium. The CFUs were counted after 16–24 h of incubation at 37 °C.

Intravital imaging of the liver, spleen and cremaster muscle

For intravital imaging, mice were anesthetized using 2.5% Avertin (300 mg/kg/mouse), comprising 0.25 g of 2,2,2-tribromethanol (Sigma) and 0.25 mL of 2-methyl-2-butanol (Sigma). Tail vein cannulation was performed to facilitate the delivery of fluorescent labeling reagents and additional anesthetics. Liver intravital imaging was executed as previously described[61]. The left lateral lobe of the liver was gently placed onto a glass coverslip integrated into the microscope stage. The coverslip was then covered with dampened Kimwipes soaked in saline solution to minimize movement. For spleen intravital imaging, the spleen was exposed onto a glass coverslip affixed to the microscope stage. Similar to the liver setup, strips of saline-moistened Kimwipes were used to prevent unnecessary motion. In the case of cremaster muscle intravital imaging, the scrotal hair was removed, and the outer skin was incised while removing excess fat. The cremaster muscle was secured using cotton thread and incised longitudinally with an electric coagulation knife. Subsequently, the cremaster muscle was laid onto a glass coverslip on the microscope stage, again utilizing saline-moistened Kimwipes to restrict movement. Images were acquired using an inverted microscope (Nikon Ti2-E) equipped with a Yokogawa CSUW1 spinning disk confocal scanner unit. Fluorescence signals were captured using the iChrome MLE compact four-color laser engine (405 nm, 488 nm, 561 nm, and 640 nm, Toptica) coupled with four specific emission filters (B447/60, B525/50, B617/73, and B685/40). Recordings were made using a sCMOS camera (Prime95B, Photometrics) that offers a substantial field of view (sensor diagonal of 18.7 mm) and high resolution (11 μm pixel size). The acquired imaging data were subsequently analyzed using either the NIS-Elements or Imaris software (version 7.0, Bitplane).

Splenectomy

Mice were anesthetized using isoflurane. The surgical site, extending from the base of the tail to the midpoint of the left ear, was shaved using a razor blade. Iodine solution was then applied to the incision area using a cotton swab. A 1 cm longitudinal incision was made in the outer skin. The inner skin was grasped with toothed forceps and incised to 0.8 cm. The spleen was carefully extracted with forceps, dissected from the surrounding fat, and the two vessels below the spleen were ligated with silk thread. The spleen was then excised using ophthalmic scissors. The fat tissue was repositioned, and the inner skin was closed with continuous sutures using hemostatic forceps. The sutured area was cleansed with iodine solution, and the outer skin was secured with a surgical skin stapler.

Flow cytometry

To isolate liver neutrophils, mouse livers were harvested, minced into small pieces, and then dissociated using the GentleMACs system. The liver homogenates were enzymatically digested in prewarmed DMEM containing 0.5 mg/mL collagenase I (Sigma) and 5 U/mL DNase I (Sigma) at 37 °C for 20 min with shaking. The digested mixture was then passed through a 200-gauge mesh. Following a brief centrifugation step to eliminate hepatocytes and tissue debris, cells were collected by pelleting and subsequently washed through centrifugation at 400 g for 5 min at 4 °C. Liver non-parenchymal cells were obtained

after lysing red blood cells with ACK buffer (Biolegend) and then were resuspended in ice-cold 1× PBS. To isolate neutrophils from bone marrow, the procedure involved aspirating bone marrow from the femurs and tibias using a syringe. The aspirated bone marrow was then gently dispersed using a pipette to ensure even distribution. Subsequently, the dispersed bone marrow was centrifuged at 400 g for 5 min at 4 °C to form a cell pellet. This pellet was treated with ACK buffer to effectively lyse red blood cells and then was resuspended in ice-cold 1× PBS. For flow cytometry analysis, a total of 1×10^6 cells were treated with Fc blocker (2.4G2, Bio X Cell) for 20 min to prevent non-specific binding. Subsequently, the cells were stained with a mixture of fluorophore-conjugated antibodies against surface markers for 30 min at 4 °C in the absence of light.

Isolation and purification of mouse and human neutrophils

Mouse neutrophils were isolated from the bone marrow using a three-layer Percoll (GE Healthcare, Cat.17-0891-09) gradient consisting of 72%, 64%, and 52%, following a previously established protocol[62]. Neutrophil purity exceeded 95%, as confirmed by the $CD45^+CD11b^+Ly6G^+$ phenotype observed in flow cytometry analysis. Similarly, human neutrophils were isolated from peripheral blood using a single-layer Ficoll-Hypaque (Tianjin Haoyang Biological Manufacture Co., Ltd, Cat. LTS1077) solution, following a previously described method[63]. Neutrophil purity exceeded 95%, as indicated by the $CD45^+CD11b^+CD15^+CD16^+$ phenotype observed in flow cytometry analysis.

Bacterial AGAR pellet Imaging

The preparation of LM-encapsulated bacterial Agar pellets was conducted as follows: Overnight cultures of LM were collected and resuspended at a concentration of 1×10^{10} CFU/mL in BHI Agar pre-warmed to 50 °C. A total of 0.1–0.5 µL of this bacterial solution was added into a 1.5 mL Eppendorf tube containing 1 mL of pre-chilled mineral oil supplemented with 1% Tween-20. Bacterial-encapsulated agar pellets were generated after a 2-h incubation on ice. Excess mineral oil was discarded, and the Eppendorf tube was topped up with cold saline. The agar pellets were then washed 5–6 times by centrifugation at 10,000 g for 5 min at 4 °C. Simultaneously, 60–65 µL of 10 mg/mL hyaluronic acid solution (Solarbio, Cat. S7020) was added to the bottom of a glass-bottom culture dish. The dish was centrifuged at 1650 g for 1 min using a spin coater to evenly spread the gel across the dish. Subsequently, 5–8 prepared bacterial agar beads were placed onto the gel, and the dish was centrifuged twice at 1650 g for 1 min to anchor the agar beads to the bottom of the dish. CFSE-labeled mouse, human neutrophils or HL-60 cells, or neutrophils isolated from Ly6G-cre-tdTomato mice (5×10^5 cells/mL) were slowly and steadily added into the dish from the sidewall to avoid disturbing the agar beads. The dish was then placed into a live-cell microscope incubation chamber (Tokai Hit) to maintain a constant temperature of 37 °C and CO_2 concentration of 5%. Time-lapse live cell images were acquired using an inverted spinning disk confocal system, as described above.

Live-cell imaging of neutrophils in vitro

Neutrophils were isolated from mouse bone marrow and resuspended to a concentration of 1×10^6 cells/mL. A total of 2 mL of this cell suspension was added to a 35 mm glass-bottom culture dish. The dish was then placed into a live-cell microscope incubation chamber (Tokai Hit) to maintain optimal conditions for cell culture. At the start of imaging, 2×10^8 CFU LM-GFP were added to the dish. PI was introduced 3 min after the start of imaging to label dead cells. For in vitro stimulation assays, a total of 5×10^5 bone marrow neutrophils were seeded into a 48 well-plate. Subsequently, 1×10^7 CFU of overnight-cultured LM was added to each well. After 1 h of stimulation, cells were harvested by centrifugation and analyzed for phagocytosis of LM using flow cytometry. The supernatant of cell culture was also collected for measurement of LTB4 production.

ELISA and ALT/AST

Blood samples were acquired through cardiac puncture or from the orbital venous plexus. Subsequently, serum was separated from the blood by centrifugation at 3000 g for 5 min. Levels of mice IFN-α (Cat. H023) and IFN-β (Cat. H024) were assessed using commercially available ELISA kits (Nanjing Jiancheng Bio. Co.), following the manufacturer's protocols. Levels of human IFN-α were assessed using commercially available ELISA kits (Dakewe, Cat. 1110012), following the manufacturer's instructions. Levels of LTB4 in neutrophil culture were assessed using commercially available ELISA kits (mlbio, Cat. ml201802), following the manufacturer's protocols. ALT (Cat. C009) and AST (Cat. C010) levels were quantified using commercially available diagnostic kits (NJJCBIO) in accordance with the manufacturer's guidelines.

Western blot

Cells were lysed using NP-40 buffer supplemented with proteinase and phosphatase inhibitor cocktails. Protein content was determined using a BCA assay, and proteins were denatured by boiling for 10–15 min in 1× sampling buffer. Proteins were then separated by SDS-PAGE. The separated proteins on the gel were transferred onto PVDF membranes, which were incubated with designated primary antibodies overnight at 4 °C. Subsequently, horseradish peroxidase (HRP)-conjugated secondary antibodies were applied and incubated with membranes for 1 h at room temperature. Chemiluminescence signals were captured using the SH-Compact 523 Imaging System from Hangzhou Shenhua Technology Co., Ltd.

Immunofluorescence

Cells were fixed using 4% paraformaldehyde, then air-dried on glass slides. Membranes were permeabilized with 0.5% Triton X-100. After an overnight incubation at 4 °C with a specific primary antibody in a humid, dark chamber, cells were washed with 1× PBS. A fluorescent secondary antibody was applied and incubated for 1 h at room temperature in a light-protected humid chamber. Following 1× PBS washing to remove the secondary antibody, DAPI staining was performed before mounting with a coverslip.

QPCR

RNA extraction and purification were conducted using the TRIzol reagent (Invitrogen) following the manufacturer's protocol. After removal of genomic DNA with gDNA Wiper (Vazyme), RNA was reverse transcribed into cDNA using the HiScript III qRT SuperMix kit (Vazyme). For semi-quantitative real-time PCR analysis of gene expression, cDNA samples were combined with primer pairs and ChamQ Universal SYBR qPCR Master Mix (Vazyme). The PCR amplification was performed using Roche LightCycler 96 instruments. The 2× Hieff PCR Master Mix (Cat. 10102) was from Yeasen. The primer list follows: *Gapdh* sense (5′-CAA CTT TGG CAT TGT GGA AGG-3′) and *Gapdh* anti-sense (5′-GAT GCA GGG ATG ATG TTC TGG-3′); *Ifnα* sense (5′-ACA TCA AAG GAC TCA TCT GC-3′) and *Ifnα* anti-sense (5′-ACA CAG TGA TCC TGT GGA AG-3′); *Ifnβ* sense (5′-AGC TCC AAG AAA GGA CGA AC-3′) and *Ifnβ* anti-sense (5′-GAA AGA CAT TCT GGA GCA TC-3′); *Alox5* sense (5′-TGG ACG TGC AAA ATT GGC CC-3′) and *Alox5* anti-sense (5′-TCG GGG CAG ATC CTT GTG GC-3′); *Cxcr2* sense (5′-CCC ATG CCA CTC AGA GAA CC-3′) and *Cxcr2* anti-sense (5′-AGA ACA GGT CAG CAA TGG CC-3′); *Fpr2* sense (5′-GGC TCA GAA CCA CCG CAC TG-3′) and *Fpr2* anti-sense (5′-ATC AGT TTG AGC CCA GGA TC-3′); human-*GAPDH* sense (5′-GTC AAG GCT GAG AAC GGG AA-3′) and human-*GAPDH* anti-sense (5′-AAA TGA GCC CCA GCC TTC TC-3′); human-*ALOX5* sense (5′-CAA CAC TAT TTC TGA GCG GG-3′) and human-*ALOX5* anti-sense (5′-GTT CCC TTG CTG GAC CTC CT−3′).

Statistical analysis

All experiments were independently replicated a minimum of two times, each with at least three biological samples per group. Statistical analyses were performed using GraphPad Prism 8.0. Results were presented as mean ± SEM. Unpaired Student's t-test was employed for pairwise comparisons between two distinct groups. For comparisons involving multiple groups, an overall one-way ANOVA followed by Dunnett's multiple comparisons test was utilized. Mouse survival was evaluated using a two-sided log-rank test. $^{*}P < 0.05$, $^{**}P < 0.01$, $^{***}P < 0.001$; ns no significance.

Reporting summary

Further information on research design is available in the Nature Portfolio Reporting Summary linked to this article.

Data availability

The authors declare that the data generated in this study are provided within the article and its Supplementary Information files. Time-lapse images presented in this study were extracted from videos. Some original videos supporting these findings are not provided due to space limitations, but are available upon request from the corresponding author if necessary. Source data are provided with this paper.

References

1. Murray, E. G. D., Webb, R. A. & Swann, M. B. R. A disease of rabbits characterised by a large mononuclear leucocytosis, caused by a hitherto undescribed bacillus *Bacterium monocytogenes* (n.sp.). *J. Pathol. Bacteriol.* **29**, 407–439 (1926).
2. Radoshevich, L. & Cossart, P. *Listeria monocytogenes*: towards a complete picture of its physiology and pathogenesis. *Nat. Rev. Microbiol.* **16**, 32–46 (2017).
3. Ebe, Y. et al. The role of Kupffer cells and regulation of neutrophil migration into the liver by macrophage inflammatory protein-2 in primary listeriosis in mice. *Pathol. Int.* **49**, 519–532 (1999).
4. Czuczman, M. A. et al. *Listeria monocytogenes* exploits efferocytosis to promote cell-to-cell spread. *Nature* **509**, 230–234 (2014).
5. Smith, G. A., Portnoy, D. A. & Theriot, J. A. Asymmetric distribution of the *Listeria monocytogenes* ActA protein is required and sufficient to direct actin-based motility. *Mol. Microbiol* **17**, 945–951 (1995).
6. Carr, K. D. et al. Specific depletion reveals a novel role for neutrophil-mediated protection in the liver during *Listeria monocytogenes* infection. *Eur. J. Immunol.* **41**, 2666–2676 (2011).
7. Nathan, C. Neutrophils and immunity: challenges and opportunities. *Nat. Rev. Immunol.* **6**, 173–182 (2006).
8. Lämmermann, T. et al. Neutrophil swarms require LTB4 and integrins at sites of cell death in vivo. *Nature* **498**, 371–375 (2013).
9. Kienle, K. et al. Neutrophils self-limit swarming to contain bacterial growth in vivo. *Science* **372**, eabe7729 (2021).
10. Pestka, S., Krause, C. D. & Walter, M. R. Interferons, interferon-like cytokines. *Immunol. Rev.* **202**, 8–32 (2004).
11. González-Navajas, J. M., Lee, J., David, M. & Raz, E. Immunomodulatory functions of type I interferons. *Nat. Rev. Immunol.* **12**, 125–135 (2012).
12. Mesev, E. V., LeDesma, R. A. & Ploss, A. Decoding type I and III interferon signalling during viral infection. *Nat. Microbiol.* **4**, 914–924 (2019).
13. Auerbuch, V., Brockstedt, D. G., Meyer-Morse, N., O'Riordan, M. & Portnoy, D. A. Mice lacking the type I interferon receptor are resistant to *Listeria monocytogenes*. *J. Exp. Med.* **200**, 527–533 (2004).
14. Stanley, S. A., Johndrow, J. E., Manzanillo, P. & Cox, J. S. The type I IFN response to infection with *Mycobacterium tuberculosis* requires ESX-1-mediated secretion and contributes to pathogenesis. *J. Immunol.* **178**, 3143–3152 (2007).
15. Henry, T. et al. Type I IFN signaling constrains IL-17A/F secretion by γδ T cells during bacterial infections. *J. Immunol.* **184**, 3755–3767 (2010).
16. Osborne, S. E. et al. Type I interferon promotes cell-to-cell spread of *Listeria monocytogenes*. *Cell. Microbiol.* https://doi.org/10.1111/cmi.12660 (2017).
17. Tan, J. M. J. et al. Listeria exploits IFITM3 to suppress antibacterial activity in phagocytes. *Nat. Commun.* **12**, 4999 (2021).
18. Rayamajhi, M., Humann, J., Penheiter, K., Andreasen, K. & Lenz, L. L. Induction of IFN-alphabeta enables *Listeria monocytogenes* to suppress macrophage activation by IFN-gamma. *J. Exp. Med.* **207**, 327–337 (2010).
19. Brzoza-Lewis, K. L., Jason Hoth, J. & Hiltbold, E. M. Type I interferon signaling regulates the composition of inflammatory infiltrates upon infection with *Listeria monocytogenes*. *Cell. Immunol.* **273**, 41–51 (2012).
20. Jia, T., Leiner, I., Dorothee, G., Brandl, K. & Pamer, E. G. MyD88 and type I interferon receptor-mediated chemokine induction and monocyte recruitment during *Listeria monocytogenes* infection. *J. Immunol.* **183**, 1271–1278 (2009).
21. McNab, F., Mayer-Barber, K., Sher, A., Wack, A. & O'Garra, A. Type I interferons in infectious disease. *Nat. Rev. Immunol.* **15**, 87–103 (2015).
22. Sheykhsaran, E., Hemmat, N. & Baghi, H. B. Influenza A virus and related secondary bacterial infections. *Rev. Med. Microbiol.* **30**, 205–211 (2019).
23. Manna, S., Baindara, P. & Mandal, S. M. Molecular pathogenesis of secondary bacterial infection associated to viral infections including SARS-CoV-2. *J. Infect. Public Health* **13**, 1397–1404 (2020).
24. Zeng, Z. T. et al. CRIg functions as a macrophage pattern recognition receptor to directly bind and capture blood-borne gram-positive bacteria. *Cell Host Microbe* **20**, 99–106 (2016).
25. Blériot, C. et al. Liver-resident macrophage necroptosis orchestrates type 1 microbicidal inflammation and type-2-mediated tissue repair during bacterial infection. *Immunity* **42**, 145–158 (2015).
26. Uderhardt, S., Martins, A. J., Tsang, J. S., Lämmermann, T. & Germain, R. N. Resident macrophages cloak tissue microlesions to prevent neutrophil-driven inflammatory damage. *Cell* **177**, 541–555.e517 (2019).
27. Dahlgren, C., Karlsson, A. & Bylund, J. Intracellular neutrophil oxidants: from laboratory curiosity to clinical reality. *J. Immunol.* **202**, 3127–3134 (2019).
28. Laleu, B. et al. First in class, potent, and orally bioavailable NADPH oxidase isoform 4 (Nox4) inhibitors for the treatment of idiopathic pulmonary fibrosis. *J. Med. Chem.* **53**, 7715–7730 (2010).
29. Castanheira, F. V. S. & Kubes, P. Neutrophils and NETs in modulating acute and chronic inflammation. *Blood* **133**, 2178–2185 (2019).
30. Li, P. et al. PAD4 is essential for antibacterial innate immunity mediated by neutrophil extracellular traps. *J. Exp. Med.* **207**, 1853–1862 (2010).
31. N, E. S. W. C. H. A. S. I. R. I. S. Enhanced resistance to *Listeria monocytogenes* in splenectomized mice. *Immunology* **33**, 851 (1977).
32. Skamene, E., Chayasirisobhon, W. & Konshavn, P. A. L. Increased phagocytic activity of splenectomized mice challenged with *Listeria monocytogenes*. *Immunology* **34**, 901–907 (1978).
33. Serbina, N. V., Shi, C. & Pamer, E. G. in *Advances in Immunology*, Vol. 113 (eds Emil, R. U. & Javier, A. C.) 119–134 (Academic Press, 2012).
34. Chakravortty, D. et al. Production of IFN-β during *Listeria monocytogenes* infection is restricted to monocyte/macrophage lineage. *PLoS One* **6**, e18543 (2011).
35. WOOD, P. R., Young, A. M., McKIMM-BRESCHKIN, J. L. & CHEERS, C. Effect of splenectomy on production of interferon and

colonystimulating factor in *Listeria monocytogenes*-infected mice. *Infect. Immun.* **46**, 860–861 (1984).
36. Zhang, G. F., Budker, V. & Wolff, J. A. High levels of foreign gene expression in hepatocytes after tail vein injections of naked plasmid DNA. *Hum. Gene Ther.* **10**, 1735–1737 (1999).
37. Hu, N. et al. A novel positive feedback loop involving FASN/p-ERK1/2/5-LOX/LTB4/FASN sustains high growth of breast cancer cells. *Acta Pharmacol. Sin.* **32**, 921–929 (2011).
38. Romerio, F., A. R. a. D. Z. Interferon-α2b reduces phosphorylation and activity of MEK and ERK through a Ras/Raf-independent mechanism. *Br. J. Cancer* **83**, 532–538 (2000).
39. Platanias, L. C. Mechanisms of type-I- and type-II-interferon-mediated signalling. *Nat. Rev. Immunol.* **5**, 375–386 (2005).
40. Song, Z., Bhattacharya, S., Clemens, R. A. & Dinauer, M. C. Molecular regulation of neutrophil swarming in health and disease: lessons from the phagocyte oxidase. *iScience* **26**, 108034 (2023).
41. Jamieson, A. M., Yu, S., Annicelli, C. H. & Medzhitov, R. Influenza virus-induced glucocorticoids compromise innate host defense against a secondary bacterial infection. *Cell Host Microbe* **7**, 103–114 (2010).
42. Manda-Handzlik, A. et al. The influence of agents differentiating HL-60 cells toward granulocyte-like cells on their ability to release neutrophil extracellular traps. *Immunol. Cell Biol.* **96**, 413–425 (2018).
43. Langford, B. J. et al. Antimicrobial resistance in patients with COVID-19: a systematic review and meta-analysis. *Lancet Microbe* **4**, e179–e191 (2023).
44. Huang, L. et al. Dynamic blood single-cell immune responses in patients with COVID-19. *Signal Transduct. Target Ther.* **6**, 110 (2021).
45. Maudet, C. et al. Bacterial inhibition of Fas-mediated killing promotes neuroinvasion and persistence. *Nature* **603**, 900–906 (2022).
46. Shi, C. et al. Ly6G+ neutrophils are dispensable for defense against systemic *Listeria monocytogenes* infection. *J. Immunol.* **187**, 5293–5298 (2011).
47. Ley, K. et al. Neutrophils new insights and open questions. *Sci. Immunol.* **3**, eaat4579 (2018).
48. Xin, L. et al. Type I IFN receptor regulates neutrophil functions and innate immunity to Leishmania parasites. *J. Immunol.* **184**, 7047–7056 (2010).
49. Stock, A. T., Smith, J. M. & Carbone, F. R. Type I IFN suppresses Cxcr2 driven neutrophil recruitment into the sensory ganglia during viral infection. *J. Exp. Med.* **211**, 751–759 (2014).
50. Lebratti, T. et al. A sustained type I IFN-neutrophil-IL-18 axis drives pathology during mucosal viral infection. *eLife* **10**, e65762 (2021).
51. Boxx, G. M. & Cheng, G. The roles of type I interferon in bacterial infection. *Cell Host Microbe* **19**, 760–769 (2016).
52. Ali, S. et al. Sources of type I interferons in infectious immunity: plasmacytoid dendritic cells not always in the driver's seat. *Front. Immunol.* **10**, 778 (2019).
53. Aoshi, T. et al. The cellular niche of *Listeria monocytogenes* infection changes rapidly in the spleen. *Eur. J. Immunol.* **39**, 417–425 (2009).
54. Jenne, Craig N. et al. Neutrophils recruited to sites of infection protect from virus challenge by releasing neutrophil extracellular traps. *Cell Host Microbe* **13**, 169–180 (2013).
55. Bai, F. et al. A paradoxical role for neutrophils in the pathogenesis of west Nile virus. *J. Infect. Dis.* **202**, 1804–1812 (2010).
56. Hawn, T. R., Wiens, K. E. & Ernst, J. D. The mechanism for type I interferon induction by *Mycobacterium tuberculosis* is bacterial strain-dependent. *PLoS Pathog.* **12**, e1005809 (2016).
57. Redford, P. S. et al. Influenza A virus impairs control of *Mycobacterium tuberculosis* coinfection through a type I interferon receptor–dependent pathway. *J. Infect. Dis.* **209**, 270–274 (2014).
58. Cillóniz, C. et al. Bacterial co-infection with H1N1 infection in patients admitted with community acquired pneumonia. *J. Infect.* **65**, 223–230 (2012).
59. Liu, Y. et al. Outcomes of respiratory viral-bacterial co-infection in adult hospitalized patients. *eClinicalMedicine*. https://doi.org/10.1016/j.eclinm.2021.100955 (2021).
60. Liu, W. et al. In situ expansion and reprogramming of Kupffer cells elicit potent tumoricidal immunity against liver metastasis. *J. Clin. Investig.* **133**, e157937 (2023).
61. Zeng, Z. et al. Sex-hormone-driven innate antibodies protect females and infants against EPEC infection. *Nat. Immunol.* **19**, 1100–1111 (2018).
62. Ubags, N. D. J. & Suratt, B. T. in *Lung Innate Immunity and Inflammation Methods in Molecular Biology*, Ch. 4, 45–57 (Springer, 2018).
63. ANDERSEN, D. Ea. B. R. SINGLE-STEP SEPARATION OF RED BLOOD CELLS. *J. Immunol. Methods* **5**, 249–252 (1974).

Acknowledgements

We thank Prof. Jianhua Li (Fudan University) for providing *Ifnar*$^{-/-}$ mice, and Prof. Xu Wang (Jiangsu University) for providing *Padi4*$^{-/-}$ mice. We also thank Prof. Wen Pan (USTC) for providing the HL-60 cell line and Prof. Rui Sun (USTC) for providing the pLive plasmid. We are grateful to Prof. Zhigang Tian (USTC), Prof. Daxing Gao (USTC), Prof. Jingren Zhang (Tsinghua University), and Prof. Weihuan Fang (Zhejiang University) for providing viral and bacterial strains. This work was funded by the National Key Research and Development Project of China (Grant# 2023YFC2306203, to Z.Z.), National Natural Science Foundation of China (NSFC) grants 82071773 and 32270958 (to Z.Z.), Research Funds of Center for Advanced Interdisciplinary Science and Biomedicine of IHM (Grant# QYPY20220001, to Z.Z.), and the USTC Research Funds of the Double First-Class Initiative (Grant# YD9100002050, to Z.Z.).

Author contributions

S.L. designed and conducted the experiments, analyzed the data, and wrote the manuscript. Q.Y. and J.L. performed some experiments. H.Y. and H.J. provided technical assistance for bacterial agar pellet imaging. R.Q. and M.Z. collected human peripheral blood samples. N.W. provided technical assistance for the L.M. infection model. L.L. and Z.Z. conceived the research, supervised the study, and edited the manuscript.

Competing interests

The authors have no conflicts of interest to declare.

Additional information

Supplementary information The online version contains supplementary material available at https://doi.org/10.1038/s41467-024-53060-4.

Correspondence and requests for materials should be addressed to Lu Li or Zhutian Zeng.

Peer review information *Nature Communications* thanks Rance Berg, Tim Lämmermann and the other, anonymous, reviewer(s) for their contribution to the peer review of this work. A peer review file is available.